In Situ Crystallization and Transformation Kinetics of Polymorphic Forms of Saturated-Unsaturated-Unsaturated Triacylglycerols: 1-palmitoyl-2,3-dioleoyl glycerol, 1-stearoyl-2,3-dioleoyl glycerol, and 1-palmitoyl-2-oleoyl-3-linoleoyl glycerol

L. Bayés-García,[a] T. Calvet,[a] M. A. Cuevas-Diarte[a] and S. Ueno[b]

[a]Departament de Cristal·lografia, Mineralogia i Dipòsits Minerals, Facultat de Geologia, Universitat de Barcelona, Martí i Franquès s/n, E-08028 Barcelona, Spain

[b]Faculty of Applied Biological Science, Hiroshima University, Higashi-Hiroshima 739, Japan

Corresponding author: Laura Bayés-García (laurabayes@ub.edu)

Abstract

We examined the influence of dynamic thermal treatment (variation of cooling/heating rates) on the polymorphic crystallization and transformation pathways of 1-palmitoyl-2,3-dioleoyl glycerol (POO), 1-stearoyl-2,3-dioleoyl glycerol (SOO), and 1-palmitoyl-2-oleoyl-3-linoleoyl glycerol (POL), which are major saturated-unsaturated-unsaturated (SUU) triacylglycerols (TAGs) of vegetable oils and animal fats (e.g., palm oil, olive oil, and Iberian ham fat). Using mainly a combination of differential scanning calorimetry (DSC) and synchrotron radiation X-ray diffraction (SR-XRD), we analyzed the polymorphic behavior of TAGs when high (15 $^{o}C \cdot min^{-1}$), intermediate (2 $^{o}C \cdot min^{-1}$), and low (0.5 $^{o}C \cdot min^{-1}$) cooling and heating rates were applied. Multiple polymorphic forms were detected in POO, SOO, and POL (sub-α, α, β'_2, and β'_1). Transient disordered phases, defined as kinetic liquid crystal (KLC) phases, were determined in POO and SOO for the first time. The results demonstrated that more stable forms were directly obtained from the melt by decreasing the cooling rates, whereas less stable forms predominated at high cooling rates, as confirmed in our previous work. Regarding heating rate variation, we confirmed that the nature of the polymorphic transformations observed (solid-state, transformation through KLC phase, or melt-mediation) depended largely on the heating rate. These results were discussed considering the activation energies involved in each process and compared with previous studies on TAGs with different saturated-unsaturated structures (1,3-dioleoyl-2-palmitoylglycerol, 1,3-dipalmitoyl-2-oleoyl-glycerol, trioleoyl glycerol, and 1,2-dioleoyl-3-linoleoyl glycerol).

Keywords: polymorphism, triacylglycerol, lipid, thermal treatment, synchrotron radiation, food product.

1. Introduction

Lipids are major nutrients and are widely employed as lipophilic materials in food, pharmaceutical, and cosmetic industries.[1] Triacylglycerols (TAGs) are the main components of natural and industrial fats and oils, and their polymorphism greatly influences the physical properties (e.g., morphology, rheology, texture, and melting) of lipid-based end products. In addition to the chemical nature of the fatty acid components (chain length, saturated/unsaturated, and cis or trans double bonds) and the connection of these fatty acids to the glycerol structure, the use of specific external factors[2,3] strongly influences the polymorphic crystallization and transformation of TAGs (e.g., the use of additives,[4] shear,[5] sonication[6-8] and emulsification[9]). In addition, applying dynamic temperature variations permits the monitoring and controlling of the polymorphic behavior of TAGs, with the aim of obtaining desired product characteristics. Many studies have been conducted to characterize the effects of dynamic temperature variation, since the kinetic properties of polymorphic crystallization and transformation of TAGs[10-16] and more complex lipid samples[17-20] are significantly influenced by cooling and heating rates. Recently, we reported on the effect of cooling rate on the polymorphic crystallization of unsaturated-saturated-unsaturated 1,3-dioleoyl-2-palmitoyl glycerol (OPO)[11] and the effects of varying both cooling and heating rates on the polymorphic crystallization and transformation pathways of saturated-unsaturated-saturated 1,3-dipalmitoyl-2-oleoyl (POP),[13] triunsaturated trioleoyl glycerol (OOO), and 1,2-dioleoyl-3-linoleoyl glycerol (OOL).[14] For that study, differential scanning calorimetry (DSC) and synchrotron radiation X-ray diffraction (SR-XRD) with small-angle (SAXD) and wide-angle (WAXD)

simultaneous measurements were used. These techniques enabled *in situ* monitoring of the occurrence of complex polymorphic transformation even when high rates (15 ºC/min) were applied.

In the present study, we used SR-XRD and DSC to dynamically follow the polymorphic crystallization and transformation kinetics of 1-palmitoyl-2,3-dioleoyl glycerol (POO), 1-stearoyl-2,3-dioleoyl glycerol (SOO), and 1-palmitoyl-2-oleoyl-3- linoleoyl glycerol (POL), which are major saturated-unsaturated-unsaturated (SUU) TAGs of lipid products (e.g., palm oil, olive oil, and Iberian ham fat).

Some previous research focused on the polymorphic characteristics of these TAGs. Miura et al.[21] studied the crystallization of POO and some POO:POP mixtures, as they play important roles in the formation of granular crystals in margarine. In addition, Zhang et al.[22] determined the eutectic binary phase behavior of POP:POO in metastable and stable conditions, due to its practical importance in dry fractionation of palm oil. In these previous studies, only two polymorphic forms (α and β') of POO were observed. Later, Zhang et al.[23] reported on the immiscible phase behavior of SOS:SOO binary mixtures, determining the presence of three SOO polymorphs (α, β'_2, and β'_1). Recently, Baker et al.[16] examined the effect of cooling rate on the polymorphism, thermal properties, and microstructure in symmetric and asymmetric TAGs containing stearic and oleic fatty acids (OSO and SOO). They observed that cooling rates have more limited effect on the phase behavior of asymmetric TAGs than on that of symmetric TAGs.

In the present work, we applied different thermal treatments to TAG samples (changing cooling/heating rates from 0.5 ºC·min^{-1} to 15 ºC·min^{-1}) to characterize

a higher number of polymorphs (sub-α, α, β'_2, and β'_1). To the best of our knowledge, this is the first time that POL polymorphism has been reported. ~~Moreover, intermediate disordered phases, defined as kinetic liquid crystal (KLC) phases, were detected in POO and SOO. The presence of some ordering in the liquid state of TAGs has been widely discussed[24-26] since Larsson first proposed the existence of liquid-crystal-like lamellae.[27,28] Ueno et al.[29] observed the liquid crystal phases of the smectic type in 1,3-distearoyl-2-oleoyl glycerol (SOS) using synchrotron radiation X-ray diffraction.~~

Considering the results of the present study as well as those of our previous work, we can compare the influence of kinetic factors (e.g., cooling/heating rates) on the polymorphic behavior observed in TAGs with different saturated-unsaturated structures (OPO, POP, OOO, OOL, POO, SOO, and POL).

2. Experimental

Samples of POO, SOO, and POL were purchased from Tsukishima Foods Industry (Tokyo, Japan) and used without further purification (purity >99%). It should be noted that the samples were not enantiopure, as they consisted of the racemic mixture of corresponding enantiomers (R and S).

DSC experiments were conducted at atmospheric pressure using both a Perkin-Elmer DSC-7 and a Perkin-Elmer DSC Diamond. The DSC thermograms obtained by the two calorimeters were comparable. Samples (9.0 to 9.4mg) were weighed into 50µl aluminum pans, and covers were sealed into place. Both instruments were calibrated with reference to the enthalpy and the melting points of indium (melting temperature 156.6 ºC; ΔH 28.45J·g^{-1}) and decane (melting

temperature -29.7 ºC; ΔH 202.1J·g^{-1}) standards. An empty pan was used as a reference. Dry nitrogen was used as purge gas in the DSC cell (at 23cm^3·min^{-1} in the Perkin-Elmer DSC-7 and at 20cm^3·min^{-1} in the Perkin-Elmer DSC Diamond). Thermograms were analyzed using Pyris Software to obtain the enthalpy (J·g^{-1}, integration of the DSC signals) and T_{onset} and T_{end} of the transitions (ºC, intersections of the baseline and the initial and final tangents at the transition). Before thermal treatments were selected, cooling and heating rate conditions were screened for POO, which was extrapolated to the SOO and POL. As we expected, the polymorphic behavior of the three TAGs was similar, due to their identical SUU structure. Thus, we carried out 16 thermal programs combining different cooling/heating rates (15 ºC·min^{-1}, 2 ºC·min^{-1}, 1 ºC·min^{-1}, and 0.5 ºC·min^{-1}; data not shown). Some of these experiment conditions were selected and more deeply characterized using SR-XRD or laboratory-scale XRD. POO, SOO, and POL samples were cooled from the melt (from 40 ºC to -80 ºC) and subsequently heated (from -80 ºC to 40 ºC) using the following rates: (1) cooling at 15 ºC·min^{-1} and heating at 15 ºC·min^{-1} and at 0.5 ºC·min^{-1}, (2) cooling at 2 ºC·min^{-1} and heating at 2 ºC·min^{-1}, and (3) cooling at 0.5 ºC·min^{-1} and heating at 15 ºC·min^{-1}. These conditions included high, intermediate and low cooling and heating rates. At least three independent measurements were performed for each experiment (n = 3). Random uncertainty was estimated with a 95% threshold of reliability using the Student's t-distribution, which enables estimating the mean of a normally distributed population when the population is small.[2430] A correction (described elsewhere[2531]) was applied for analyses with cooling or heating rates other than 2 ºC·min^{-1}, since both calorimeters were calibrated at this rate.

Formatted: Superscript

Formatted: Superscript

SR-XRD experiments were performed at the beamline BL-9C of the synchrotron radiation facility Photon Factory (PF) of the High-Energy Accelerator Research Organization (KEK) in Tsukuba (Japan). A double-focusing camera was operated at a wavelength of 0.15nm. X-ray scattering data were simultaneously collected using Position Sensitive Proportional Counters (PSPCs) (Rigaku Co., PSPC-10) for small (SAXD) and wide (WAXD) angles. The SAXD pattern was used for determining the chain length structure of the TAG, and the WAXD pattern permitted us to identify the polymorphic forms. Each temperature program was controlled using a Linkam stage LK-600. A 2mm-thick sample was placed in an aluminum sample cell with Kapton film windows. SR-XRD spectra were acquired at 30 or 60s intervals, depending on the cooling/heating rates used and the complexity of the thermal profile.

Laboratory-scale powder XRD was used for some experiment conditions using a PANalytical X'Pert Pro MPD powder diffractometer equipped with a Hybrid Monochromator and an X'Celerator Detector. The equipment also included an Oxford Cryostream Plus 220V (temperature 80 to 500K). This diffractometer operated with Debye-Scherrer transmission. The sample was introduced in a 1mm-diameter Lindemann glass capillary. The latter was rotated about its axis during the experiment to minimize preferential orientations of the crystallites. The step size was 0.013º from 1.004º to 28º 2θ, and the measuring time was 2.5min per pattern.

3. Results

Table 1 summarizes the long and short spacings of the observed POO, POL, and SOO polymorphs. These values are in good agreement with those of previous studies.[21-23]

Table 1. Long and short spacing values of the POO, POL and SOO polymorphs.

POO		
	Long Spacing/nm	Short Spacing/nm
sub-α	5.8 2.9	0.42 0.38
α	5.7 2.8	0.41
KLC	6.0	—
β'_2	6.7 3.2	0.43 0.41
β'_1	6.7 3.2	0.47 0.46 0.45 0.43 0.41 0.40 0.39
POL		
	Long Spacing/nm	Short Spacing/nm
sub-α	5.7 2.8	0.42 0.38
α	5.6 2.7	0.41
β'_2	6.3 3.1	0.42 0.38
β'_1	6.4 3.1	0.47 0.46 0.45 0.44 0.42 0.41 0.40 0.39
SOO		
	Long Spacing/nm	Short Spacing/nm
sub-α	6.2 3.0	0.42 0.38
α	6.0 2.9	0.41
KLC	6.7	—
β'_2	7.1 3.4	0.43 0.41
β'_1	6.9 3.3	0.47 0.45 0.43 0.42 0.41 0.40 0.39

Chain length structures of sub-α and α forms are double, and those for the two β' forms are triple. Long spacings become much greater than those of POP and OPO, especially for double chain length structures, as the inclination angles toward the lamellar interface should be relatively small. KLC forms were formed in POO and SOO, and they were characterized by a single long spacing (see below).

3.1. Polymorphic characteristics of 1-palmitoyl-2,3-dioleoyl glycerol

Table 2 presents DSC data (T_{onset} and ΔH) of all the thermal treatments applied to POO. At high (15 ºC·min^{-1}) and intermediate (2 ºC·min^{-1}) cooling rates, the crystallizing polymorph was α, whereas low rates (0.5 ºC·min^{-1}) led to more stable forms (β'$_2$). With heating, the most stable form (β'$_1$) was obtained in all cases, but through different pathways depending on the rate used.

Table 2. DSC data of crystallization and transformation of POO polymorphs obtained by cooling rates of (A) 15 ºC·min^{-1}, (B) 2 ºC·min^{-1}, and (C) 0.5 ºC·min^{-1} and different heating rates. The letters, *c* and *m*, in parentheses noting polymorph forms mean crystallization and melting.

A	**Cooling (15 ºC·min^{-1})**		**Heating (15 ºC·min^{-1})**				
	α (c)	*α → sub-α*	*sub-α → α*	*α (m)*	*β'$_2$ (c)*	*β'$_2$ → β'$_1$*	*β'$_1$ (m)*
T_{onset} (ºC)	-20.4 ± 0.4	-62.9 ± 0.5	-65.8 ± 0.5	-44.0 ± 2.1	-16.3 ± 0.4	-6.6 ± 0.6	12.5 ± 0.5
ΔH (J/g)	-44 ± 1	-5 ± 1	9 ± <1	4 ± 1	-29 ± 1	-17 ± 2	111 ± 3
			(0.5 ºC·min^{-1})				
			sub-α⇒β'$_1$	*β'$_1$ (m)*			
T_{onset} (ºC)			3.5 ± 2.3	12.4 ± 0.3			
ΔH (J/g)			(T_{end}) ___	106 ± 21			
B	**Cooling (2 ºC·min^{-1})**		**Heating (2 ºC·min^{-1})**				
	α (c)	*α → sub-α*	*sub-α⇒β'$_1$*	*β'$_1$ (m)*			
T_{onset} (ºC)	-11.3 ± 1.6	___	-0.8 ± 3.7	13.5 ± 0.9			
ΔH (J/g)	-78 ± 2	___	(T_{end}) ___	109 ± 8			
C	**Cooling (0.5 ºC·min^{-1})**		**Heating (15 ºC·min^{-1})**				
	β'$_2$+β'$_1$ (c)		*β'$_2$ (m)*	*β'$_1$ (m)*			
T_{onset} (ºC)	7.3 ± 1.3		-4.5 ± 4	14.4 ± 1.5			
ΔH (J/g)	-103 ± 4		1 ± <1	108 ± 5			

Figure 1 depicts the polymorphic behavior of POO when cooled at 15 ºC·min^{-1} and heated at 15 ºC·min^{-1} and 0.5 ºC·min^{-1}.

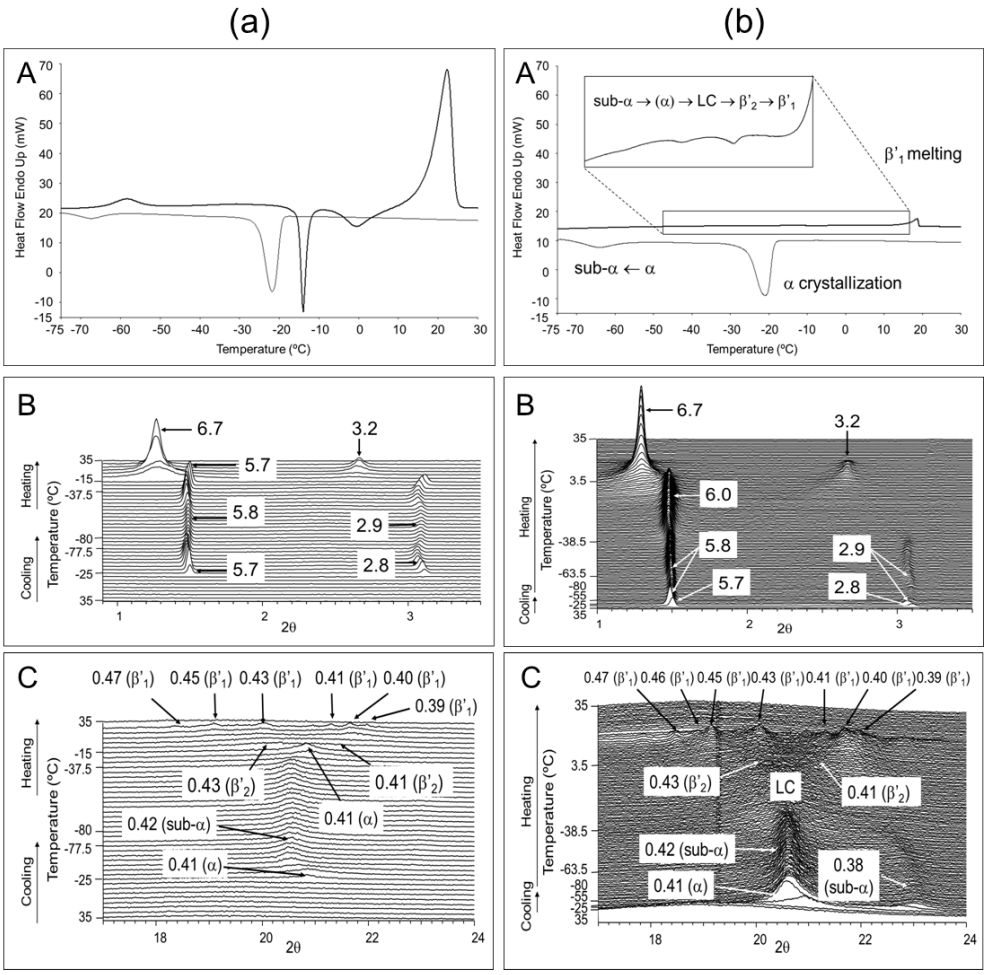

Fig. 1. Polymorphic behavior of POO. (a) Cooling at 15 ºC·min^{-1} and heating at 15 ºC·min^{-1}. A. DSC thermogram. B. SR-SAXD pattern. C. SR-WAXD pattern. (b) Cooling at 15 ºC·min^{-1} and heating at 0.5 ºC·min^{-1}. A. DSC thermogram. B. SR-SAXD patern. C. SR-WAXD patern.

When the molten POO sample was cooled at 15 ºC·min^{-1}, the crystallizing polymorph was α, with a long spacing of 5.7nm and a short spacing of 0.41nm. On further cooling, the SR-XRD peaks shifted from 5.7 to 5.8nm (SAXD pattern) and from 0.41 to 0.42nm (WAXD pattern), due to α→sub-α transformation. This sub-α form was characterized by two WAXD peaks (a stronger one at 0.42nm accompanied by a weaker one at 0.38nm), which was not observed at high

cooling/heating rates but could be determined with other experiment conditions (see WAXD pattern in Fig. 1b). When POO was subsequently heated at 15 ºC·min^{-1} (Fig. 1a), sub-α→α transformation occurred at -65.8 ºC (Table 2A); according to SR-XRD, the SAXD peak at 5.8nm moved to 5.7nm, and the WAXD peak at 0.42nm shifted to 0.41nm. Here, α form melted at -44.0ºC and β'$_2$ form crystallized at -16.3 ºC, detected by the presence of the SAXD peak at 6.7nm and two broad WAXD peaks at 0.43 and 0.41nm. Later, the DSC profile indicated an exothermic peak at -6.6 ºC, corresponding to a β'$_2$→β'$_1$ transition. Simultaneously, new WAXD peaks appeared at 0.47, 0.45, 0.43, 0.41, and 0.40nm; however, the SAXD peak at 6.7nm did not change. Finally, according to the DSC data, the most stable form (β'$_1$) melted at 12.5 ºC. The considerable width and the high enthalpy of the β'$_1$ melting peak (111 J·g^{-1}) may be the result of concurrent melting of both β'$_2$ and β'$_1$ forms that may have occurred due to the high heating rate used.

In contrast, when the POO sub-α form was heated at a low rate (0.5 ºC·min^{-1}) (Fig. 1b), a series of complex thermal phenomena was observed in the DSC thermogram at a temperature range of -50 to 3.5 ºC (enlarged figure in Fig. 1b). Because the endothermic/exothermic nature of the DSC peaks could not be properly identified, only the T_{end} of this set of phenomena was determined (Table 2A, in which the process is noted as sub-α⇒β'$_1$). Throughout this large temperature range, the SR-XRD data indicated that the SAXD peak at 5.8nm shifted to 6.0nm and its corresponding (002) reflection did not appear. Regarding the WAXD pattern, the typical peak of sub-α form at 0.42nm vanished, and no diffraction peak was present. This disordered phase, having a single long spacing, could be interpreted as a KLC phase. This phase is characterized by a structural

periodicity of 6.0nm of lamellar distance but with no definite periodicity in lateral packing. The presence of some ordering in the liquid state of TAGs has been widely discussed[26-28] since Larsson first proposed the existence of liquid-crystal-like lamellae.[29,30] Other studies that reported liquid crystal phases in other TAGs (e.g., 1,3-distearoyl-2-oleoyl glycerol (SOS)[29~~30~~31]) defined them as a smectic LC. Many transitions were observed in this wide temperature range, and the sequence probably passed through some α form before the formation of KLC. Furthermore, the DSC data did not indicate any clear peak corresponding to KLC formation, as it was somehow overlapped in the complex set of phenomena in the temperature range corresponding to the sub-α⇒β'_1 transformations. Later, KLC transformed to β'_2 form (presence of a SAXD peak at 6.7nm and two WAXD peaks at 0.43 and 0.41nm); then $\beta'_2 \rightarrow \beta'_1$ transition occurred. Thus, the typical SR-XRD peaks of β'_1 forming at 0.47, 0.46, 0.45, 0.43, 0.41, 0.40, and 0.39nm were observed in the WAXD pattern. Finally, β'_1 form melted at 12.4 ºC.

Intermediate cooling and heating rates were also applied (2 ºC·min^{-1}). The polymorphic behavior observed was the same as that obtained by cooling at 15 ºC·min^{-1} and heating at 0.5 ºC·min^{-1} (Fig. 2 and Table 2B).

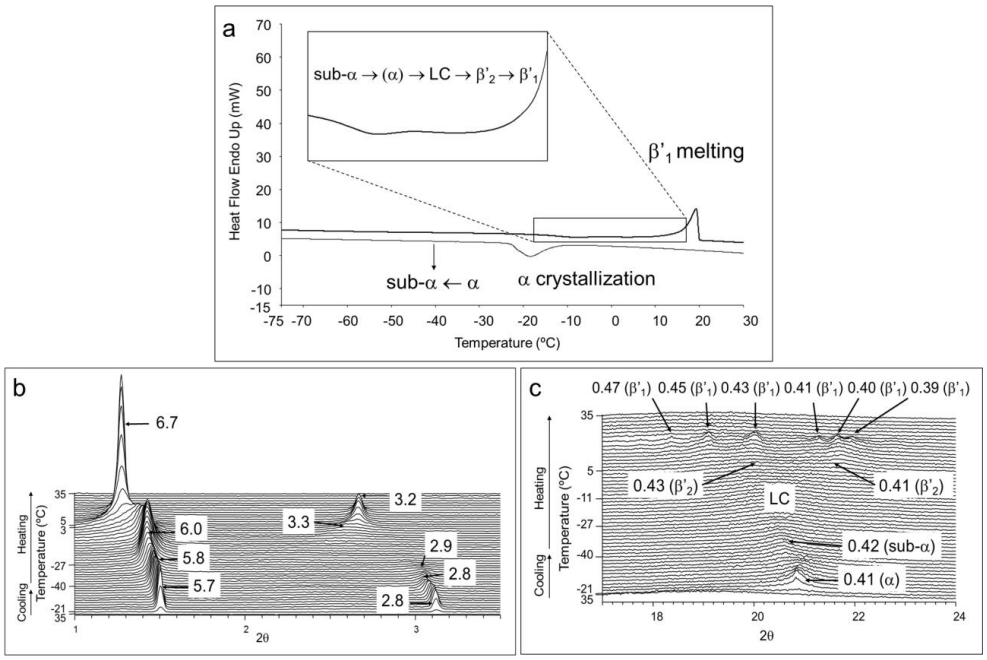

257

258 **Fig. 2.** Polymorphic behavior of POO when cooled at 2 ºC·min^{-1} (α crystallization) and heated at 2
259 ºC·min^{-1}. a) DSC thermogram. b) SR-SAXD pattern. c) SR-WAXD pattern.

260

261 Hence, when cooling at 2 ºC·min^{-1}, the DSC thermogram indicated an exothermic
262 peak with a T_{onset} at -11.3 ºC corresponding to the α form crystallization
263 (identifiable by a SAXD peak at 5.7nm and a WAXD peak at 0.41nm).
264 Furthermore, the SR-XRD data indicated a shift from 5.7 to 5.8nm in the SAXD
265 pattern and from 0.41 to 0.42nm in the WAXD pattern, due to the α→sub-α
266 transformation, although no corresponding DSC thermal peak was observed.
267 After POO was cooled at 2 ºC·min^{-1}, it was heated at the same rate. Again, a
268 complicated transformation process appeared in the DSC heating curve over a
269 wide temperature range (-20 to -0.8 ºC). The SAXD pattern again indicated a
270 single peak at 6.0nm and no WAXD peak was detected, corresponding to the
271 KLC phase described above. Immediately afterwards, the β'_2 form could be

identified by the presence of the SAXD peak at 6.7nm and two peaks at 0.43 and 0.41nm in the WAXD pattern. Finally, β'_2 form transformed to β'_1 form, and the WAXD peaks shifted to 0.47, 0.45, 0.43, 0.41, 0.40, and 0.39nm. β'_1 form melted at 13.5 ºC (Table 2B), with the ΔH value of 109J·g^{-1}.

The polymorphic crystallization of POO was also studied at low cooling rates. Thus, the melted sample was cooled at 0.5 ºC·min^{-1} and heated at 15 ºC·min^{-1} (Fig. 3).

Conventional XRD could be carried out under these conditions, due to the simplicity observed in the DSC thermal profile. β'_2 and β'_1 forms crystalized concurrently at 7.3 ºC (Table 2C).

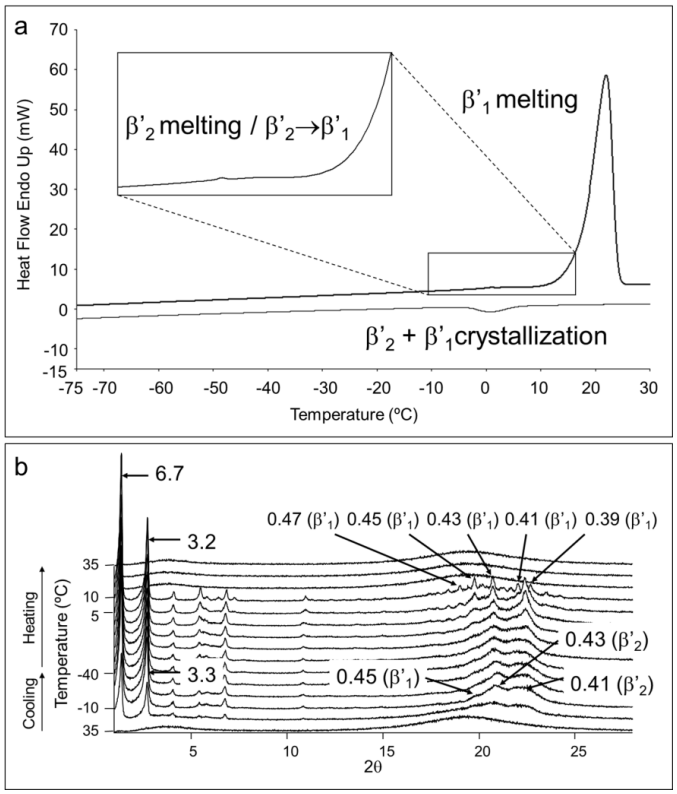

Fig. 3. Polymorphic behavior of POO when cooled at 0.5 ºC·min^{-1} (β'_2 + β'_1 crystallization) and heated at 15 ºC·min^{-1}. a) DSC thermogram. b) Conventional XRD paterns.

The XRD pattern exhibited a peak at 6.7nm in the small-angle region and three peaks in the wide-angle XRD region at 0.45nm (corresponding to β'_1 form), and 0.43 and 0.41nm (β'_2 form). On heating, the DSC curve exhibited a weak and broad melting peak with T_{onset} at -4.5 ºC. In the same temperature range, the XRD patterns indicated more defined β'_1 peaks (0.47, 0.45, 0.43, 0.41, and 0.39nm); thus, this broad DSC peak was probably due to some β'_2 melting, some $\beta'_2 \rightarrow \beta'_1$ transition, or a combination of the two. Finally, only β'_1 form was present, and it melted at 14.4 ºC.

3.2. Polymorphic Characteristics of 1-palmitoyl-2-oleoyl-3-linoleoyl glycerol

1-palmitoyl-2-oleoyl-3-linoleoyl glycerol (POL) was subjected to the same thermal treatments, and the polymorphic behavior was similar to that of POO. Table 3 presents T_{onset} and ΔH values of the phenomena observed in the corresponding DSC thermograms.

Table 3. DSC data of crystallization and transformation of POL polymorphs obtained by cooling rates of (A) 15 ºC·min^{-1}, (B) 2 ºC·min^{-1}, and (C) 0.5 ºC·min^{-1} and different heating rates. The letters, *c* and *m*, in parentheses noting polymorph forms mean crystallization and melting.

A	**Cooling (15 ºC·min^{-1})**		**Heating (15 ºC·min^{-1})**				
	α (c)	*α → sub-α*	*sub-α → α*	*α (m)*	*β'$_2$ (c)*	*β'$_2$ → β'$_1$*	*β'$_1$ (m)*
T_{onset} (ºC)	-20.6 ± 0.3	-41.3 ± 0.6 (peak top)	-31.8± 1.6 (peak top)	-16.1 ± 1.7	-12.6 ± 2.3	-5.6 ± 2	8.8 ± 2.2
ΔH (J/g)	-45 ± 2	-1 ± 1	2 ± 1	22 ± 4	-85 ± 18		97 ± 8
			(0.5 ºC·min^{-1})				
			sub-α → α	*α → β'$_2$*	*β'$_2$ → β'$_1$*	*β'$_2$ (m)*	*β'$_1$ (m)*
T_{onset} (ºC)			-35.2 ± 2.5 (peak top)	-33.7 ± 1.2	-10.4 ±1.3	8.2 ± 0.5	9.6 ± 0.3
ΔH (J/g)			12 ± 2	-18 ± 2	-6 ± 2	14 ± 3	93 ± 4
B	**Cooling (2 ºC·min^{-1})**		**Heating (2 ºC·min^{-1})**				
	α (c)	*α → sub-α*	*α → β'$_2$*	*β'$_2$ → β'$_1$*	*β'$_2$ (m)*	*β'$_1$ (m)*	
T_{onset} (ºC)	-17.5 ± 0.6	-36.3 ± 0.6 (peak top)	-23.0 ± 0.7	-6.0 ± 1.1	7.5 ± 0.8	10.1 ± 0.8	
ΔH (J/g)	-45 ± 2	-1 ± 1	-24 ± 2	-12 ± 9	107 ± 9		
C	**Cooling (0.5 ºC·min^{-1})**		**Heating (15 ºC·min^{-1})**				
	β'$_2$ (c)		*β'$_2$ (m)*	*β'$_1$ (c)*	*β'$_1$ (m)*		
T_{onset} (ºC)	-12.8 ± 0.9		-1.5 ± 1.2	1.6 ± 1.6	8.0 ± 1.2		
ΔH (J/g)	-79 ± 10		3 ± 2	-17 ± 2	99 ± 5		

Not surprisingly, α form was crystallized from the melt at high and intermediate rates (15 and 2 ºC·min^{-1}), whereas a more stable β'$_2$ form was obtained at low cooling rates (0.5 ºC·min^{-1}). Heating resulted in a polymorphic sequence of increasing stability; however, no KLC phase was detected.

Figures 4a and 4b depict the polymorphic behavior of POL observed when the molten sample was cooled at 15 ºC·min^{-1} and heated at 15 and 0.5 ºC·min^{-1}.

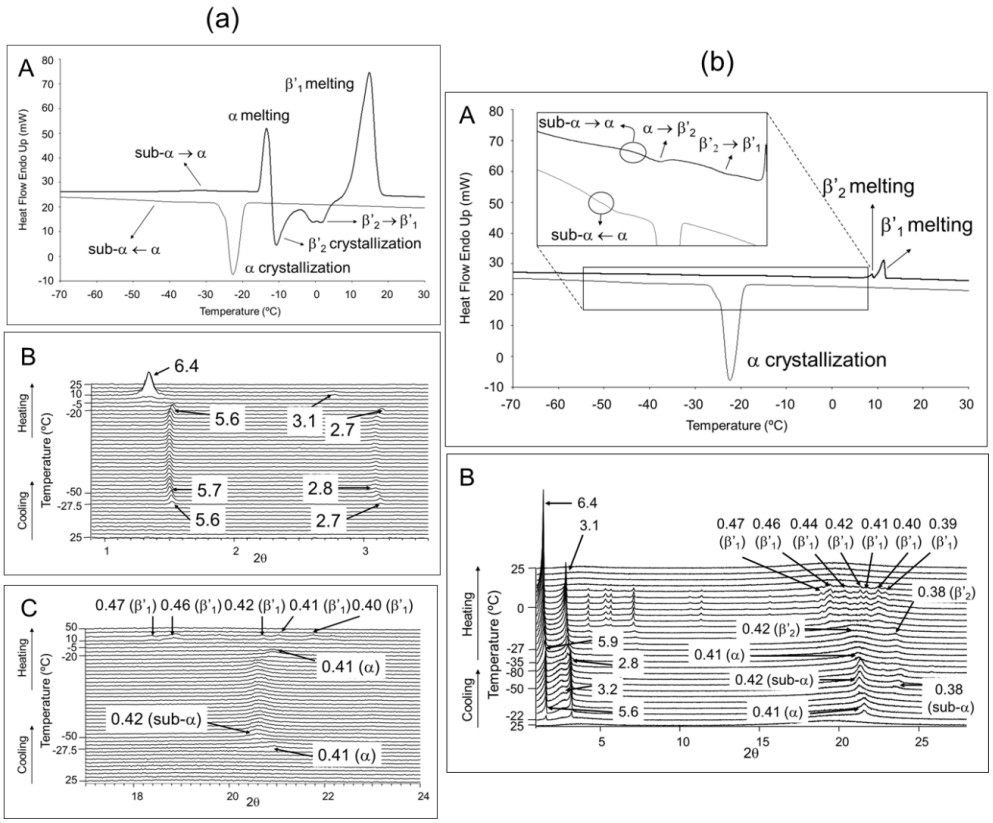

Fig. 4. Polymorphic behavior of POL. (a) Cooling at 15 ºC·min^{-1} and heating at 15 ºC·min^{-1}. A. DSC thermogram. B. SR-SAXD pattern. C. SR-WAXD pattern. (b) Cooling at 15 ºC·min^{-1} and heating at 0.5 ºC·min^{-1}. A. DSC thermogram. B. Conventional XRD patterns.

When the molten POL sample was cooled at 15 ºC·min^{-1}, SR-XRD data indicated α form crystallization, which occurred at -20.6 ºC, through a SAXD peak at 5.6nm and a WAXD peak at 0.41nm. As depicted in Fig. 4a, shifting to 5.7nm and 0.42nm resulted in α→sub-α transformation, corresponding to a DSC peak top at -41.3 ºC. However, T_{onset} could not be determined, due to the flatness of the DSC peak. The opposite polymorphic transformation (sub-α→α) occurred at -31.8 ºC (peak top) when heating; simultaneously, the SAXD peak at 5.7nm moved to 5.6nm again, and the WAXD peak moved from 0.42 to 0.41nm. A

sharp endothermic DSC signal appeared at -16.1 ºC, corresponding to the α melting, and further on, crystallization occurred. Two exothermic peaks (with T_{onset} at -12.6 ºC and at -5.6 ºC) appeared; however, only the latest could be identified. SR-XRD indicated β'_1 form through the peaks at 6.4nm (SAXD) and at 0.47, 0.46, 0.42, 0.41, and 0.40nm (WAXD). Similar to POO, the exothermic DSC peak with T_{onset} at -12.6 ºC was probably due to the β'_2 crystallization, which transformed to β'_1 form at -5.6 ºC. However, the two processes could not be distinguished using SR-XRD, as they were so close to each other and the heating rate used was so high. Finally, β'_1 form melted at 8.8 ºC.

Figure 4b depicts the DSC and laboratory-scale XRD results obtained when POL was cooled at 15 ºC·min^{-1} and heated at 0.5 ºC·min^{-1}. Heating at such a low rate transformed the sub-α form obtained during cooling to α form at -35.2 ºC (peak top temperature, see Table 3A), which soon changed to β'_2 form through exothermic solid-state transformation at -33.7 ºC. β'_2 form was identified by its wide-angle region peaks at 0.42 and 0.38nm, as the laboratory-scale XRD data indicated. Again, the most stable polymorph of POL (β'_1) was reached on further heating, when an exothermic peak, corresponding to the $\beta'_2 \rightarrow \beta'_1$ transition, appeared at -10.4 ºC in the DSC profile. The XRD peaks at 6.4nm (small-angle) and 0.47, 0.46, 0.44, 0.42, 0.41, 0.40, and 0.39nm (wide-angle region) indicated the presence of β'_1 form. Finally, two consecutive melting peaks were observed in the DSC heating curve, corresponding to both melting processes of remaining β'_2 (T_{onset} = 8.2ºC) and β'_1 (T_{onset} = 9.6ºC) forms. Hence, not all the existing β'_2 form was transformed to β'_1 at -10.4 ºC.

With intermediate cooling/heating rates (2 ºC·min^{-1}), the polymorphic behavior of POL did not exhibit significant variation. As depicted in Fig. 5, α crystals were also obtained by cooling the melted sample at 2 ºC·min^{-1}, which, according to the DSC data, transformed to sub-α form at -36.3 ºC (Table 3B). This transition was identified in the SR-XRD pattern by the shift from 5.6 to 5.7nm (SAXD) and from 0.41 to 0.42 and 0.38nm.

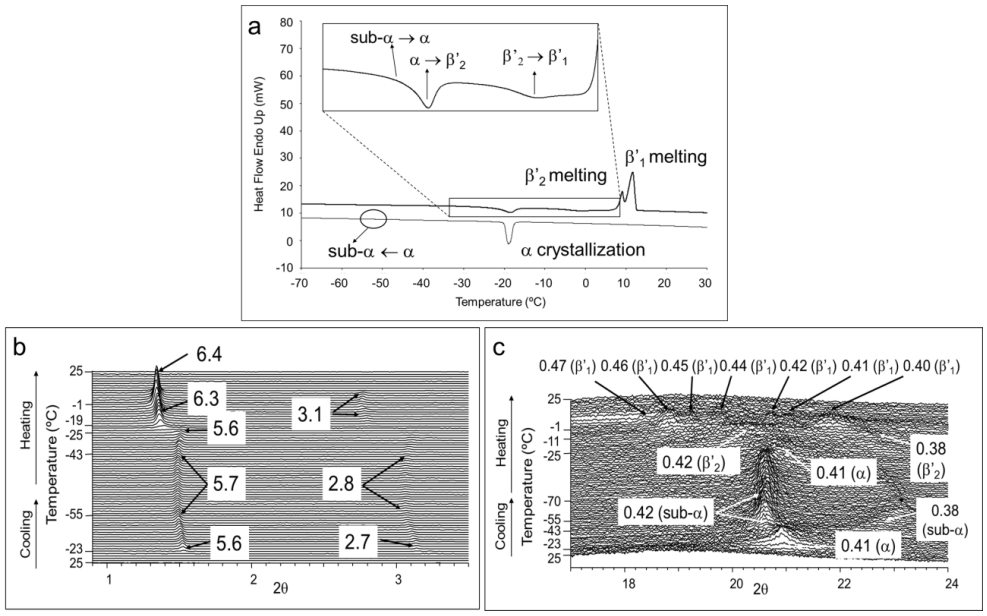

Fig. 5. Polymorphic behavior of POL when cooled at 2 ºC·min^{-1} (α crystallization) and heated at 2 ºC·min^{-1}. a) DSC thermogram. b) SR-SAXD pattern. c) SR-WAXD patern.

During heating, although no corresponding DSC peak was observed, sub-α transformed to α form (the SAXD peak at 5.6nm and the WAXD peak at 0.41 appeared again at the expense of α peaks). Soon afterward, a SAXD peak at 6.3nm and two WAXD peaks at 0.42 and 0.38nm appeared at -23.0 ºC, indicating solid-state transformation from α to β'$_2$ form. Part of this β'$_2$ transformed to β'$_1$

374 form at -6.0 ºC, indicated by the SAXD peak at 6.4nm and typical WAXD peaks
375 at 0.47, 0.46, 0.45, 0.44, 0.42, 0.41, and 0.40nm. Finally, β'$_2$ form melted at 7.5
376 ºC, and β'$_1$ form melted at 10.1 ºC. Unlike the results obtained with low heating
377 rates (0.5 ºC·min^{-1}) for POL, the two endothermic melting peaks were not
378 completely separated at 2 ºC·min^{-1}, and the melting enthalpy (107 J·g^{-1}) had to be
379 determined as a whole (the sum of the two melting processes).
380 More stable β'$_2$ crystallization occurred when melted POL was cooled at 0.5
381 ºC·min^{-1}. Figure 6 presents the DSC and SR-XRD data for cooling at 0.5 ºC·min^{-1}
382 and heating at 15 ºC·min^{-1}.
383

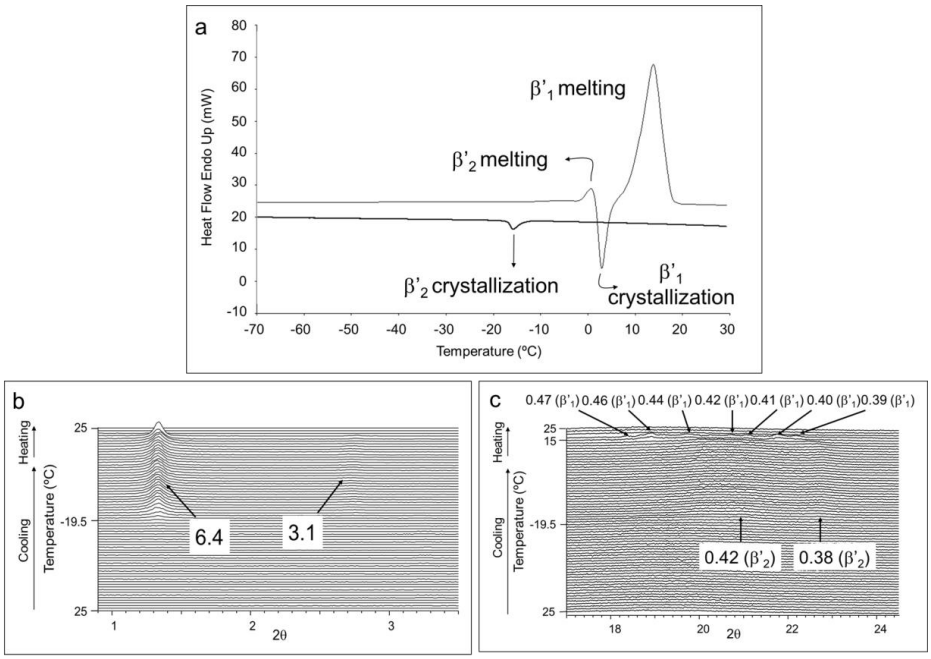

384

385 **Fig. 6.** Polymorphic behavior of POL when cooled at 0.5 ºC·min^{-1} (β'$_2$ crystallization) and heated at 15
386 ºC·min^{-1}. a) DSC thermogram. b) SR-SAXD pattern. c) SR-WAXD pattern.
387

388 β'$_2$ form was identified by a triple chain length SAXD peak at 6.4 and two broad
389 WAXD peaks at 0.42 and 0.38nm. When the sample was quickly heated at 15

390 ºC·min^{-1}, melt-mediated transformation from β'$_2$ to β'$_1$ form occurred, consisting
391 of β'$_2$ melting (T_{onset} at -1.5ºC) and β'$_1$ crystallization at 1.6ºC (Table 3C). During
392 this transformation, the SAXD peak did not change, whereas WAXD peaks
393 appeared at 0.47, 0.46, 0.44, 0.42, 0.41, 0.40, and 0.39nm, at the expense of β'$_2$
394 peaks. The most stable β'$_1$ form melted at 8 ºC. The considerable width of the
395 endothermic peak may be due to some concurrent β'$_2$ and β'$_1$ melting.

396

397 **3.3. Polymorphic Characteristics of 1-stearoyl-2,3-dioleoyl glycerol**

398

399 The influence of varying the cooling and heating rates was also analyzed for 1-
400 stearoyl-2,3-dioleoyl glycerol (SOO). Table 4 presents the DSC data of all the
401 thermal peaks observed.

402

403 **Table 4.** DSC data of crystallization and transformation of SOO polymorphs obtained by cooling rates of
404 (A) 15 ºC·min^{-1}, (B) 2 ºC·min^{-1}, and (C) 0.5 ºC·min^{-1} and different heating rates. The letters, *c* and *m*, in
405 parentheses noting polymorphic forms mean crystallization and melting.

A	**Cooling (15 ºC·min^{-1})**		**Heating (15 ºC·min^{-1})**				
	α (c)	*α → sub-α*	*sub-α → α*	*α (m)*	*β'$_2$ (c)*	*β'$_2$ →β'$_1$*	*β'$_1$ (m)*
T_{onset} (ºC)	-9.0 ± 0.4	-25.0 ± 0.3	-22.4 ± 0.8	-6.2 ± 0.9	-3.3 ± 0.6	2.7 ± 0.8	19.8 ± 0.5
ΔH (J/g)	-48 ± 1	-1 ± <1	1 ± 1	7 ± 2	-74 ± 16		109 ± 9
			(0.5 ºC·min^{-1})				
			sub-α → α	*α → β'$_2$*	*β'$_2$ → β'$_1$*	*β'$_1$ (m)*	
			-62.2 ± 1.4	-26.6 ± 0.7	-4.5 ± 0.6	22.0 ± 0.6	
			9 ± 8	-18 ± 4	-3 ± 1	136 ± 18	
B	**Cooling (2 ºC·min^{-1})**		**Heating (2 ºC·min^{-1})**				
	α + β'$_2$(c)	*α → sub-α*	*KLC → β'$_2$*	*β'$_2$ → β'$_1$*	*β'$_1$ (m)*		
T_{onset} (ºC)	-5.4 ± 0.3	-21.8 ± 0.6	-18.9 ± 0.9	-2.4 ± 0.4	20.9 ± 0.4		
ΔH (J/g)	-49 ± 3	-1 ± <1	-21 ± 1	-15 ± 2	122 ± 4		
C	**Cooling (0.5 ºC·min^{-1})**		**Heating (15 ºC·min^{-1})**				
	β'$_2$ (c)		*β'$_2$ → β'$_1$*	*β'$_1$ (m)*			

T_{onset} (ºC)	5.5 ± 1.8	6.5 ± 1.6	21.1 ± 1.0
ΔH (J/g)	-96 ± 4	-15 ± 6	111 ± 10

406

407

408 Following the same tendency as POO and POL, metastable α form crystallized at
409 high cooling rates, while α and β'_2 forms crystallized concurrently at intermediate
410 rates, and β'_2 crystals were obtained at low rates. Forms of increasing stability
411 were reached while heating similar to POO, and a KLC phase was identified in
412 some experiment conditions.
413 When cooling SOO at 15 ºC·min^{-1}, exothermic crystallization of α form occurred
414 at -9.0 ºC, and transformation to sub-α form occurred at -25.0 ºC. Thus, the
415 SAXD peak moved from 6.0nm (α) to 6.2nm (sub-α), and the α WAXD peak at
416 0.41nm changed to the two sub-α peaks at 0.42 and 0.38nm. An exothermic peak
417 was observed at -70 ºC, and an endothermic peak was observed at the beginning
418 of the heating step at 15 ºC·min^{-1} (at -60 ºC) (Fig. 7a) in the DSC profile.
419 However, they could not be identified using the SR-XRD patterns, as no changes
420 were detected in these temperature ranges. On further heating, sub-α form
421 transformed to α form at -22.4 ºC. Immediately afterward, melt-mediated
422 transformation occurred from α to β'_2 form, which consisted of α form melting
423 (at -6.2 ºC) and subsequent β'_2 crystallization (at -3.3 ºC). Simultaneously, SR-
424 XRD peaks became very flat, almost nonexistent, due to the α melting; a triple
425 chain length SAXD peak at 7.1nm and two broad β'_2 WAXD peaks progressively
426 appeared at 0.43 and 0.40nm, as a result of the β'_2 crystallization. Furthermore,
427 the peak at 7.1nm, observable in the SAXD pattern, moved to 6.9nm; new

WAXD peaks at 0.45, 0.43, and 0.40nm identified $\beta'_2 \rightarrow \beta'_1$ solid-state transformation, which occurred at 2.7 ºC. β'_1 form melted at a T_{onset} of 19.8 ºC.

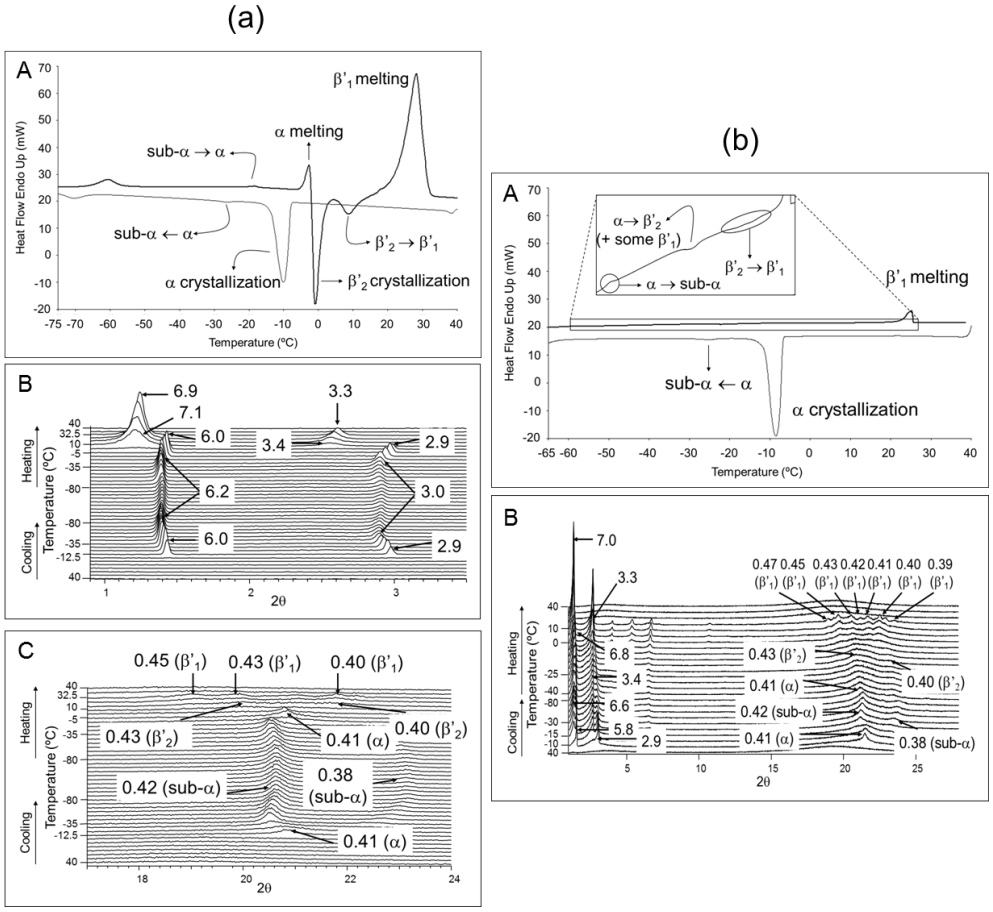

Fig. 7. Polymorphic behavior of SOO. (a) Cooling at 15 ºC·min^{-1} and heating at 15 ºC·min^{-1}. A. DSC thermogram. B. SR-SAXD pattern. C. SR-WAXD pattern. (b) Cooling at 15 ºC·min^{-1} and heating at 0.5 ºC·min^{-1}. A. DSC thermogram. B. Conventional XRD patterns.

Figure 7b depicts the DSC and laboratory-scale XRD data obtained by cooling SOO at 15 ºC·min^{-1} and heating at 0.5 ºC·min^{-1}. Heating the sub-α form at such a low rate resulted in transformation to α form at -62.2 ºC (Table 4A and enlarged

440 figure in Fig. 7(b) A). At -26.6 ºC, a α→β'$_2$ transition was identified by the two
441 typical broad XRD peaks at 0.43 and 0.40nm in the wide-angle region. Later,
442 another transformation (from β'$_2$ to β'$_1$ form) occurred at -4.5 ºC. At this point,
443 β'$_1$ XRD peaks appeared at 0.47, 0.45, 0.43, 0.42, 0.41, 0.40, and 0.39nm. This
444 most stable form finally melted at 22.0 ºC, with a melting enthalpy of 136J·g^{-1}.
445 This high value suggests that, as expected, low heating rates produce higher
446 amounts of the most stable forms. However, taking into account the low enthalpy
447 associated with the β'$_2$→β'$_1$ transformation (-3 J·g^{-1}), one may reasonably assume
448 that some β'$_1$ form was formed in another step, such as in the α→β'$_2$ transition.
449 Therefore, some β'$_1$ form may have formed concurrently with β'$_2$. Analysis of the
450 XRD patterns indicated that the β'$_2$ diffraction peaks became so broad that they
451 were probably overlapping some β'$_1$ peaks, which became more defined on
452 further heating when all SOO was converted into β'$_1$ form.
453 Intermediate cooling and heating rates (2 ºC·min^{-1}) were also applied to SOO
454 (Fig. 8).
455

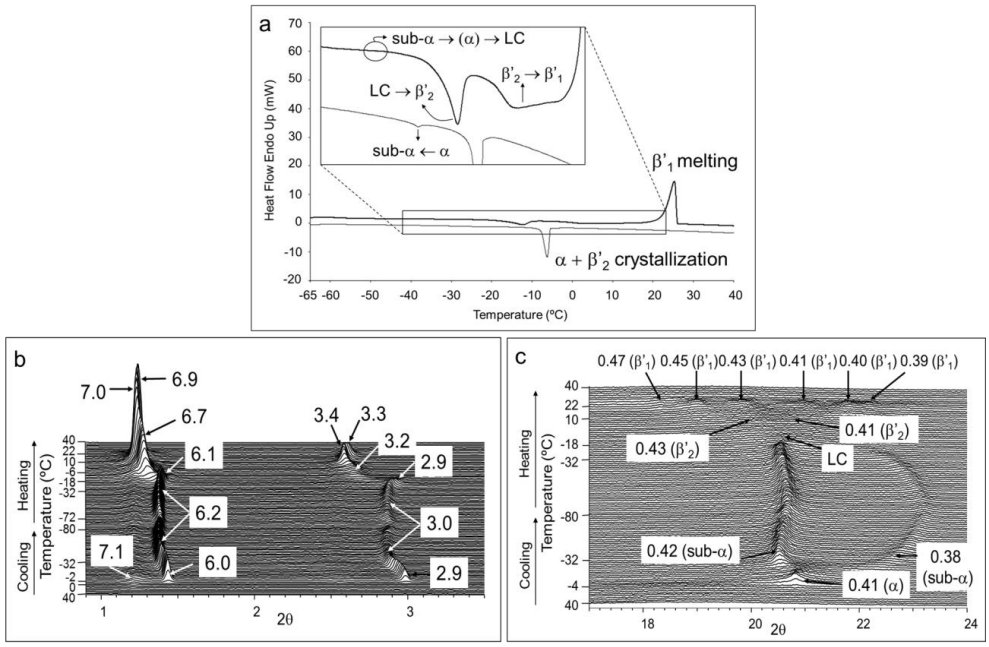

Fig. 8. Polymorphic behavior of SOO when cooled at 2 °C·min^{-1} (α + β'$_2$ crystallization) and heated at 2 °C·min^{-1}. (a) DSC thermogram. (b) SR-SAXD pattern. (c) SR-WAXD pattern.

Concurrently, α and β'$_2$ forms crystallized from the melt at -5.4 °C when the sample was cooled at 2 °C·min^{-1}. Thus, the SR-SAXD pattern indicated the presence of a weak peak at 7.1nm (corresponding to β'$_2$ form) and another one at 6.0nm (corresponding to α form). However, the SR-WAXD pattern exhibited the α peak only at 0.41nm. At -21.8 °C, the SAXD peak moved to 6.2nm, and the WAXD peak at 0.41nm split into two peaks at 0.42nm and 0.38nm, due to the α→sub-α transformation. Later, when the sub-α form was heated at 2 °C·min^{-1}, diffraction peaks disappeared in the WAXD pattern and a single SAXD peak was detected at 6.1nm, indicating the KLC phase, similar to POO. Nevertheless, this phenomenon could not be attributed to any thermal peak of the DSC curve. Judging from the long spacings, some α form probably formed before the KLC phase, because a weak SAXD peak at 2.9nm, corresponding to the 002 reflection

of the α peak at 6.0nm, could be observed. On further heating, the SAXD peak β'$_2$ form appeared at 7.0nm, and WAXD peaks appeared at 0.43 and 0.41nm. The exothermic DSC peak at -18.9 ºC could be attributed to this KLC→β'$_2$ transition. However, because of the complexity and lack of clarity in the DSC data, interpretation of these phenomena was based mainly on the SR-XRD results. According to the DSC data, β'$_2$ form transformed to β'$_1$ form at -2.4 ºC. The SR-XRD then indicated a shift from 7.0nm to 6.9nm; and new WAXD peaks appeared at 0.47, 0.45, 0.43, 0.41, 0.40, and 0.39nm. Soon after β'$_1$ formed, it melted at 20.9 ºC.

Simpler polymorphic behavior was verified by cooling molten SOO at 0.5 ºC·min^{-1} and heating it at 15 ºC·min^{-1} (Fig. 9).

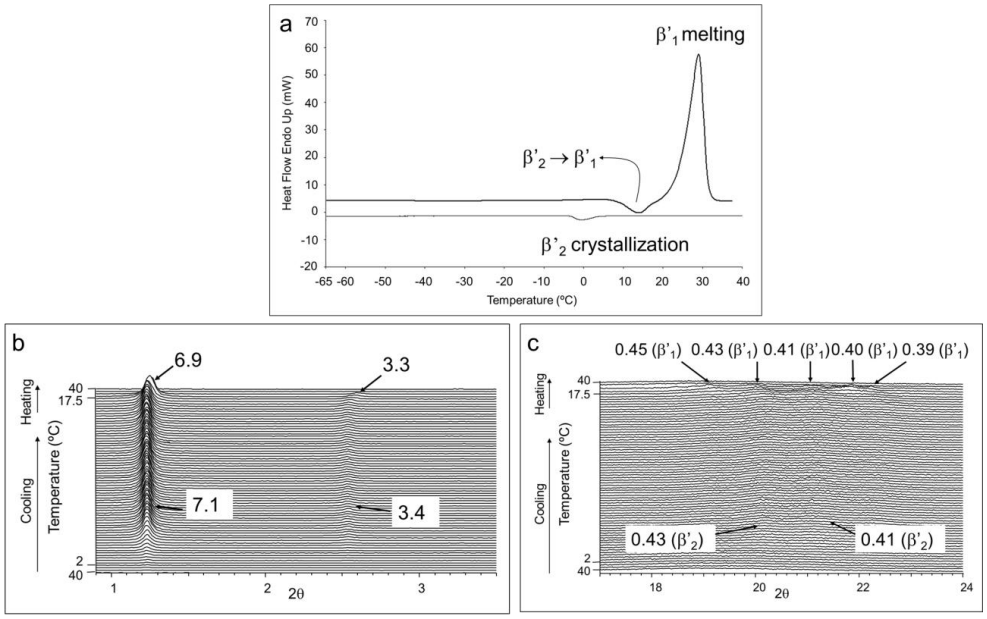

Fig. 9. Polymorphic behavior of SOO when cooled at 0.5 ºC·min^{-1} (β'$_2$ crystallization) and heated at 15 ºC·min^{-1}. a) DSC thermogram. b) SR-SAXD pattern. c) SR-WAXD pattern.

488

489 At this low cooling rate, β'_2 crystals were obtained from the melt at 5.5 ºC (Table
490 4C), as confirmed by the SR-XRD data, with a SAXD peak at 7.1nm, and two
491 WAXD peaks at 0.43 and 0.41nm. When heating, the DSC curve exhibited an
492 exothermic phenomenon at 6.5 ºC, corresponding to the $\beta'_2 \rightarrow \beta'_1$ transformation.
493 SR-XRD data enabled us to identify the β'_1 form through the diffraction peaks at
494 6.9nm (SAXD pattern), and at 0.45, 0.43, 0.41, 0.40, and 0.39nm. According to
495 the DSC results, β'_1 form melted at 21.1 ºC.

496

497

498

499

500

501 **4. Discussion**

502

503 **4.1. Polymorphic behavior of POO, POL, and SOO**

504

505 The three SUU TAGs described in this work exhibited very similar polymorphic
506 crystallization and transformation pathways when different cooling and heating
507 rates were applied.
508 Figure 10 depicts some schematic diagrams of the polymorphic pathways
509 followed by the mentioned compounds as a summary.

510

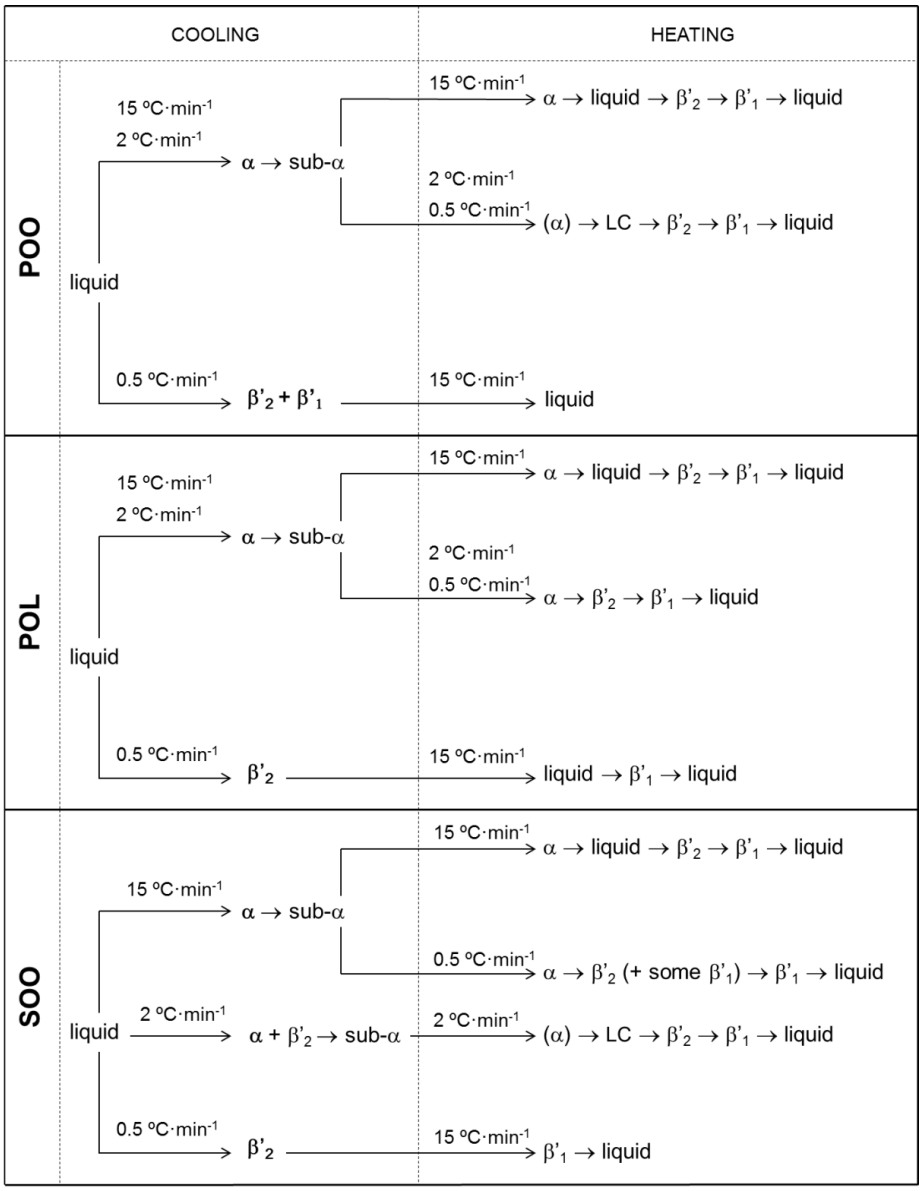

511

512 **Fig. 10.** Diagrams of polymorphic pathways of POO, POL and SOO under different cooling and heating

513 conditions.

514

515 ~~The polymorphic behavior of POO, POL, and SOO when samples were cooled~~

516 ~~and heated at 15°C·min^{-1} was the same in all three cases: α crystals were directly~~

517 ~~obtained from the melt, and they transformed to sub-α form on further cooling.~~

518 ~~Upon heating, the sequence of polymorphic transformation was sub-~~

~~α →α →liquid →β'$_2$ →β'$_1$ →liquid. However, when sub-α crystals were heated at low rates (0.5ºC·min^{-1}), complex DSC curves were obtained in all cases, with the general pattern of sub-α →α →β'$_2$ →β'$_1$ →liquid. In this sequence of polymorphic transformation, a KLC phase was detected between α and β'$_2$ forms in POO, but not for POL or SOO. In general terms, the difference between the pathways observed using high and low heating rates lies in the nature of the α →β'$_2$ transformation: melt-mediation at 15ºC·min^{-1} and solid-state at 0.5ºC·min^{-1}. These results were quite similar to those observed in 1,3-dipalmitoyl-2-oleoyl glycerol (POP),[13] trioleoyl glycerol (OOO), and 1,2-dioleoyl-3-linoleoyl glycerol (OOL).[14]~~

~~At intermediate cooling/heating rates (both 2ºC·min^{-1}), the results obtained for POO and POL were the same as those of cooling at 15ºC·min^{-1} and heating at 0.5ºC·min^{-1}. In contrast, α and β'$_2$ forms crystallized concurrently in SOO, instead of only α form. Heating of these polymorphic forms at 2ºC·min^{-1} resulted in the sequence of sub-α →(α) →KLC →β'$_2$ →β'$_1$ →liquid. We specified α form in parentheses, as some α form (α 002 peak at 2.9nm) may have occurred for a short time before the KLC phase. Here, we should point out the formation of the KLC phase when POO was cooled at 15ºC·min^{-1} and heated at 0.5ºC·min^{-1}, and cooled and heated at 2ºC·min^{-1}. For SOO, the KLC phase was observed only when it was cooled and heated at 2ºC·min^{-1}, not when it was cooled at 15ºC·min^{-1} and heated at 0.5ºC·min^{-1}.~~

~~Finally, the three samples were subjected to a low cooling rate (0.5ºC·min^{-1}) and a high heating rate (15ºC·min^{-1}). As expected, more stable forms than α crystallized from the melt, not following the Ostwald step rule of stages:[32] β'$_2$ form in POL and SOO, and concurrent β'$_2$+β'$_1$ forms in POO. With high heating~~

~~rates, β'$_2$ form transformed to β'$_1$, which finally melted. However, the nature of this polymorphic transformation differed for the three TAGs: it occurred through melt-mediation in POL and through solid-state in SOO. For POO, no clear transformation appeared in the DSC heating curve.~~

4.2. Comparison of POO, POL, SOO, OPO, POP, OOO, and OOL polymorphisms

Following the same tendencies as those observed in OPO,[11] POP,[13] OOO, and OOL,[14] the present study demonstrated the following crystallization and transformation properties, which are strongly related to the thermal treatments applied:

(1) Four polymorphic forms (sub-α, α, β'$_2$, and β'$_1$) were isolated in POO, POL, and SOO. Furthermore, KLC phases were observed in POO and SOO.

(2) More stable polymorphs were directly obtained from the melt, not following the Ostwald step rule of stages[32], by decreasing the cooling rates, whereas less stable forms predominated at high cooling rates.

(3) Higher amounts of the most stable form (β'$_1$) were obtained by decreasing the heating rate. Also, with low heating rates, solid-state transformations occurred more easily at the expense of melt-mediated transformations.

These properties were also observed for OPO, POP, OOO, and OOL using DSC and SR-XRD when different thermal treatments were applied. Table 5 summarizes the crystallization and transformation pathways of POP, OPO, POO, POL, SOO, OOO, and OOL at different cooling and heating rates.

Table 5. Crystallization and transformation pathways of POP, OPO, POO, POL, SOO, OOO and OOL at different cooling and heating rates, in which *mm* and *ss* mean melt-mediated and solid-state transformations.

		POP	OPO	POO	POL	SOO	OOO	OOL
Polymorphs		α-2, γ-3, β'-2, δ-3, β-3	α-2, β'-2 , β-3	sub-α-2, α-2, KLC, β'-3	sub-α-2, α-2, β'-3	sub-α-2, α-2, KLC, β'-3[a]	α-2, β'-2 , β-2	α-2, β'-2
Crystallization on cooling	rapid	α	α	α	α	α	α	α
	slow	γ	β' + β	β'	β'	β'	β'	β'
Transformation on heating	rapid	α→(*mm*)β'→L γ→L	α→(*mm*) β'→β→L β'→β→L	α→(*mm*)β'→L β'→L	α→(*mm*)β'→L β'→L	α→(*mm*)β'→L β'→L	α→(*mm*) β'→(*mm*) β→L β'→(*mm*) β→L	α→(*mm*) β'→L β'→L
	slow	α→γ→(*ss*)δ→(*mm*) β→L γ→(*mm*) β'+δ→(*mm*) β→L	n.a[b] n.a[b]	α→KLC→β'→L n.a[b]	α→(*ss*)β'→L n.a[b]	α→KLC→β'→L n.a[b]	n.a[b] β'→(*ss*) β→L	α→(*ss*) β'→L β'→L

[a] For simplicity, β_2' and β_1' or β_2 and β_1 are summarized into β' or β, respectively.

[b] Not available.

Regarding polymorphic crystallization by changing the cooling rates, multiple polymorphic forms involving the most stable β form were obtained with the unsaturated-saturated-unsaturated OPO, demonstrating complex concurrent crystallization in most cases. For triunsaturated OOO and OOL, and saturated-unsaturated-unsaturated POO, POL, and SOO (present work), α was crystallized with rapid cooling, whereas β' was obtained with slow cooling. However, for the saturated-unsaturated-saturated POP, it was difficult to obtain stable forms such as β' and β even when the cooling rate was lowered to 0.5 $^{o}C \cdot min^{-1}$.

When the heating rate was ~~varied~~ changed, more stable polymorphic forms (e.g., β' and β) were obtained either through solid-state or melt-mediation for OPO, OOO, OOL, POO, POL, and SOO even at a high rate (15 $^{o}C \cdot min^{-1}$). However, it was necessary to decrease the heating rates to 2 to 0.1 $^{o}C \cdot min^{-1}$ to obtain the most stable β form for POP. Thus, we may conclude that similar polymorphic crystallization and transformation characteristics were obtained in OPO, OOO, OOL, POO, POL, and SOO; however, POP differed in the difficulty of obtaining the most stable β form.

The present study has also proposed a new transformation pathway through the occurrence of KLC phases in POO and SOO (both SUU TAGs) when intermediate (2 $^{o}C \cdot min^{-1}$) and/or low (0.5 $^{o}C \cdot min^{-1}$) heating rates were used. Thus, lamellar structures having lamellar distances of 6.0nm were identified in POO and those having that of 6.7nm were identified in SOO, with no definite periodicity in lateral packing. This result indicates that, according to Ueno et al.,[31~~29~~] both KLC phases may correspond to smectic liquid crystals. This is the first work reporting KLC phases for POO and SOO. However, no KLC phases were detected for the other TAGs examined under any cooling/heating

602 conditions. The two KLC phases occurred in the sequence α-2→KLC→β'-3.
603 Ueno et al.[31,29] determined two different LC phases (LC1 and LC2) for SOS using
604 SR-XRD. However, they did not monitor the cooling and heating rates, as the
605 thermal treatments used consisted of controlled temperature jumps and annealing
606 steps. Similar to the results obtained in our work, Ueno et al. confirmed LC1
607 formation for SOS during the melt-mediation of α to obtain β' crystals. However,
608 with a jump to a higher temperature, they observed a new type of liquid crystal
609 (LC2) during the intermediate period after the α melting and before the
610 occurrence of γ and β'. For SOS and our case study (POO and SOO), LC phases
611 became transitory states between a double-chain-length structure (α form) and a
612 triple-chain-length structure (β' form), which could be monitored using SR-XRD.
613 In other words, KLC phases may be needed for the mentioned TAGs to transform
614 from a 2L (α) to a 3L (β') structure with the experiment conditions used.
615 However, this transitory KLC phase was not necessary for other 2L→3L
616 transformations, as confirmed in previous work on POP and OPO.
617 Our experiment results indicated that quick heating (15 ºC·min^{-1}) of α crystals
618 results in melt-mediated transformation of SOO to obtain β'_2 form
619 (α→liquid→β'_2) (Fig. 10). As expected, with a low heating rate (0.5 ºC·min^{-1}),
620 this transformation occurred in the solid state (α→β'_2). However, with an
621 intermediate heating rate (2 ºC·min^{-1}), and similar to the work described by Ueno
622 et al.,[31,29] a KLC phase occurred between α and β'_2. Melt-mediated transformation
623 from α to β'_2 was also detected when α POO crystals were heated at 15 ºC·min^{-1},
624 and an intermediate KLC phase occurred between these two polymorphic forms
625 when heating at 2 ºC·min^{-1} and 0.5 ºC·min^{-1}. Thus, we conclude that we may use

Formatted: Superscript

626 a lower heating rate (less than 0.5 ºC·min^{-1}) for POO to observe α→β'$_2$ solid-state
627 transformation. No KLC phase appeared for POL in any of the experiment
628 conditions. With heating at 15 ºC·min^{-1}, melt-mediation occurred from α to β'$_2$,
629 whereas this transformation took place in the solid state when heated at 2 and 0.5
630 ºC·min^{-1}. Thus, the transient KLC phase may be observed using an intermediate
631 heating rate (15 to 2 ºC·min^{-1}). In all cases, KLC phases were detected only when
632 using SR-XRD, not laboratory-scale XRD. However, KLC phases were
633 observable within wide temperature ranges during heating; thus, we assume that
634 laboratory-scale XRD may also be capable of detecting them.
635
636 **4.3. Thermodynamic properties of polymorphic transformations of POO,**
637 **POL, and SOO compared to OPO, POP, OOO, and OOL**
638
639 As discussed in our previous work,[13] these results may be interpreted considering
640 the activation energies of solid-state and melt-mediated transformations from a
641 less stable polymorphic form to a more stable form (Fig. 11).
642

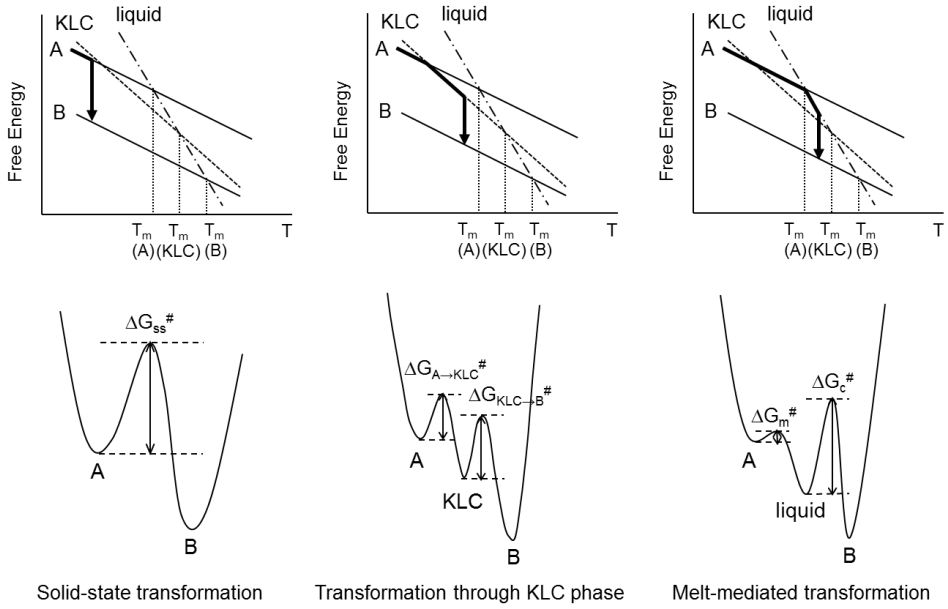

643

644 **Fig. 11.** Activation free energy ($\Delta G^{\#}$) for solid-state transformation, transformation through KLC phase,
645 and melt-mediated transformation from metastable A to more stable B forms.

646

647 Transformation rates are determined by the magnitude of the activation free
648 energies ($\Delta G^{\#}$) involved in each process. In solid-state transformation from form
649 A to form B, $\Delta G_{ss}^{\#}$ may include excess energy to enable structural changes, such
650 as changes in the subcell structure and chain length structure. However, in melt-
651 mediated transformation, the rate may be determined by the magnitude of $\Delta G_m^{\#}$
652 (melting of form A) and the subsequent crystallization ($\Delta G_c^{\#}$) of form B.
653 However, the actual rate may be determined by $\Delta G_c^{\#}$ due to the ease of melting
654 and the low values of $\Delta G_m^{\#}$.
655 One may simply assume that the $\Delta G_{ss}^{\#}$ values for transformation involving
656 change from loosely packed subcell structures (e.g., hexagonal subcell of α form)
657 to more closely packed subcell structures of $O_{\perp}$ (β') and $T_{//}$ (β) are larger than
658 those involving change from $O_{\perp}$ (β') to $T_{//}$ (β). Also, $\Delta G_{ss}^{\#}$ values may be lower

659 for transformation between polymorphs having the same double-chain-length
660 structures (e.g., α→β' in OPO and α→β' in OOO and OOL) than for changes
661 from double- to triple-chain-length structures (e.g., α→ β' in POO, SOO, and
662 POL; α→γ and β'→β in POP) (Fig. 12). The same assumption may apply to
663 crystallization, in that the $\Delta G_c^{\#}$ values of polymorphs having tightly packed
664 subcell and triple-chain-length structures (e.g., β form of OPO or POP) may
665 exceed those of others.
666

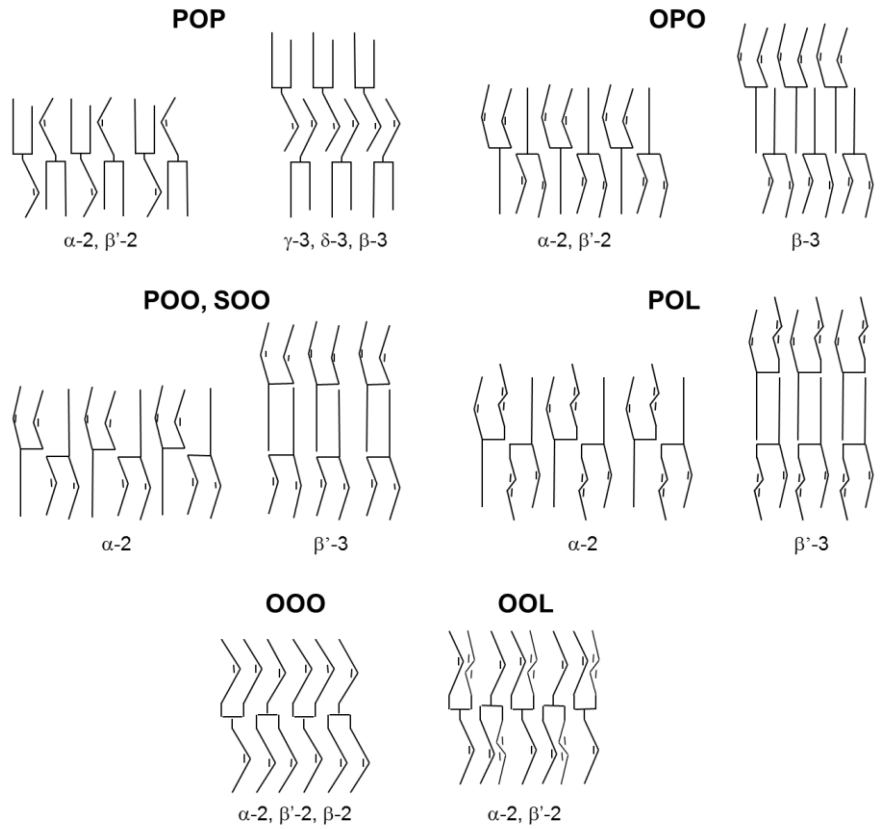

667

668 **Fig. 12.** Structure models of POP, OPO, POO, SOO, POL, OOO and OOL. For simplicity, multiple β'
669 and β forms are represented by β' and β.

670

As depicted in Fig. 11, KLC formation was observed at intermediate heating rates between solid-state and melt-mediated transformation, so that the $\Delta G^{\#}$ value involved in transformation through the KLC phase may be lower than that of solid-state transformation but higher than that of melt-mediation. KLC phase was kinetically detected as a transient state between less stable form A and more stable form B, so that, as illustrated in Figure 11, its melting temperature may be higher than that of A but lower than that of B. According to Figure 11, we considered that the transformation from A to KLC phase occurred at a temperature below T_m(A), as no clear subsequent crystallization phenomena was determined from SR-XRD data. However, one may consider that KLC phase was observed within wide temperature range in all cases.

POP exhibited a peculiar polymorphic behavior compared to that of the other TAGs examined: even during slow heating, solid-state transformation occurred with more difficulty. This difference may be due to the fact that POP contains more saturated fatty acid moieties (palmitic acid) whose transformation from less stable to more stable forms may need larger activation energy ($\Delta G_{ss}^{\#}$) than TAGs containing more unsaturated fatty acid moieties. The flexibility of the chain packing of unsaturated acids is more enhanced than that of saturated fatty acids,[33] which may decrease the value of $\Delta G_{ss}^{\#}$ for transformation into more stable forms in more unsaturated TAGs. This may also apply to the difficulty for POP to obtain stable polymorphic forms from the melt, even with low cooling rates.

The SUU TAGs analyzed in this study also exhibited a particular behavior due to intermediate KLC phases, which were not detected in POP, OPO, OOO, or OOL using the same experiment conditions. These KLC phases occurred within $\alpha \rightarrow \beta'_2$ transformation, which involves rearrangement from a double-chain-length

696 structure (α) to a triple-chain-length structure (β'_2). The KLC phases in these
697 SUU TAGs may be due to some lateral disorder caused by a mismatch in
698 molecule packing, which may be more important in asymmetric TAGs than in
699 symmetric TAGs.[15] Baker et al. found that, when comparing the polymorphic
700 behavior of symmetric OSO and asymmetric SOO, the lateral disorder, probably
701 generated by local defects in the packing of the molecules, may be amplified by
702 the asymmetrical position of the two flexible non-oriented unsaturated chains.
703
704 **5. Conclusions**
705
706 The application of dynamic thermal treatments is closely related to actual
707 crystallization processes of edible fats. This study examined the occurrence and
708 transformation pathways of polymorphic forms of POO, POL, and SOO as a
709 function of cooling and heating rate variations. The results obtained were
710 compared to those of previous studies on other TAGs (OPO, POP, OOO, and
711 OOL) and were discussed in terms of activation free energy and molecular
712 structure. A peculiar polymorphic behavior was observed in POO, POL, and
713 SOO, which exhibited KLC phase formation as a transient state in transformation
714 from polymorphic forms having a double-chain-length structure to polymorphs
715 with a triple-chain-length structure.
716
717 **Acknowledgements**
718
719 The authors acknowledge the financial support of the Ministerio de Economía y
720 Competitividad through Project MAT2011-27225. SR-XRD experiments were

721 conducted with the approval of the Photon Factory Program Advisory Committee
722 (proposals 2010G114, 2010G656, and 2012G704). The authors gratefully
723 appreciate the help of Prof. Masaharu Nomura, Station Manager of BL-9C at the
724 Photon Factory. The authors also acknowledge the Generalitat de Catalunya
725 through the Grup Consolidat 2014SGR1208.

726

727 **References**

728 1. Larsson, K., Quinn, P., Sato, K. & Tiberg, F. (Eds.) (2006). *Lipids:*
729 *structure, physical properties and functionality*. Bridgewater: The Oily
730 Press.
731 2. Sato, K., Bayés-García, L., Calvet, T., Cuevas-Diarte, M. A. & Ueno, S.
732 (2013). External factors affecting polymorphic crystallization of lipids.
733 *European Journal of Lipid Science and Technology, 115*, 1224-1238.
734 3. Bayés-García, L., Patel, A. R., Dewettinck, K., Rousseau, D., Sato, K. &
735 Ueno, S. (2015). Lipid crystallization kinetics – roles of external factors
736 influencing functionality of end products. *Current Opinion in Food*
737 *Science*, *4*, 32-38.
738 4. Smith, K. W., Bhaggan, K., Talbot, G. & van Malssen, K. F. (2011).
739 Crystallization of Fats: Influence of Minor Components and Additives.
740 *Journal of the American Oil Chemists' Society, 88*, 1085-1101.
741 5. Mazzanti, G., Li, M., Marangoni, A. G. & Idziak, S. H. J. (2011) Effects
742 of Shear Rate Variation on the Nanostructure of Crystallizing
743 Triglycerides. *Crystal Growth & Design*, *11*, 4544-4550.

Formatted: *Spanish (Spain, International Sort)*

744 6. Ueno, S., Ristic, R. I., Higaki, K. & Sato, K. (2003). In Situ Studies of
745 Ultrasound-Stimulated Fat Crystallization Using Synchrotron Radiation
746 *Journal of Physical Chemistry B, 107*, 4927-4935.
747 7. Chen, F., Zhang, H., Sun, X., Wang, X. & Xu, X. (2013). Effects of
748 Ultrasonic Parameters on the Crystallization Behavior of Palm Oil.
749 *Journal of the American Oil Chemists' Society*, *90*, 941-949.
750 8. Ye, Y. & Martini, S. (2015). Application of High-Intensity Ultrasound to
751 Palm Oil in a Continuous System. *Journal of Agricultural and Food*
752 *Chemistry*, *63*, 319-327.
753 9. Wassell, P., Okamura, A., Young, N. W. G., Bonwick, G., Smith, C., Sato,
754 K. & Ueno, S. (2012). Synchrotron Radiation Macrobeam and Microbeam
755 X-ray Diffraction Studies of Interfacial Crystallization of Fats in Water-in-
756 Oil Emulsions. *Langmuir, 28*, 5539-5547.
757 10. Smith, K. W., Cain, F. W. & Talbot, G. (2005). Crystallization of 1,3-
758 dipalmitoyl-2-oleoylglycerol and tripalmitoylglycerol and their mixtures
759 from acetone. *European Journal of Lipid Science and Technology*, *107*,
760 583-593.
761 11. Bayés-García, L., Calvet, T., Cuevas-Diarte, M. A., Ueno, S. & Sato, K.
762 (2011). *In situ* synchrotron radiation X-ray diffraction study of
763 crystallization kinetics of polymorphs of 1,3-dioleoyl-2-palmitoyl glycerol
764 (OPO). *CrystEngComm, 13*, 3592-3599.
765 12. Bouzidi, L. & Narine, S. S. (2012). Relationships between molecular
766 structure and kinetic thermodynamic controls in lipid systems. Part II:
767 Phase behavior and transformation paths of SSS, PSS and PPS saturated

768 triacylglycerols – Effect of chain length mismatch. *Chemistry and Physics*
769 *of Lipids, 165,* 77-88.
770 13. Bayés-García, L., Calvet, T., Cuevas-Diarte, M. A., Ueno, S. & Sato, K.
771 (2013). *In situ* observation of transformation pathways of polymorphic
772 forms of 1,3-dipalmitoyl-2-oleoyl glycerol (POP) examined with
773 synchrotron radiation X-ray diffraction and DSC. *CrystEngComm, 15,*
774 302-314.
775 14. Bayés-García, L., Calvet, T., Cuevas-Diarte, M. A., Ueno, S. & Sato, K.
776 (2013). Crystallization and Transformation of Polymorphic Forms of
777 Trioleoyl Glycerol and 1,2-Dioleoyl-3-*rac*-linoleoyl Glycerol. *Journal of*
778 *Physical Chemistry B, 117,* 9170-9181.
779 15. Baker, M., Bouzidi, L., Garti, N. & Narine, S. S. (2014). Multi-length-
780 Scale Elucidation of Kinetic and Symmetry Effects on the Behavior of
781 Stearic and Oleic TAG. I. SOS and SSO. *Journal of the American Oil*
782 *Chemists' Society, 91,* 559-570.
783 16. Baker, M. R., Bouzidi, L., Garti, N. & Narine, S. S. (2014). Multi-Length-
784 Scale Elucidation of Kinetic and Symmetry Effects on the Behavior of
785 Stearic and Oleic TAG. II: OSO and SOO. *Journal of the American Oil*
786 *Chemists' Society, 91,* 1685-1694.
787 17. Lopez, C., Lesieur, P., Bourgaux, C. & Ollivon, M. (2005). Thermal and
788 Structural Behavior of Anhidrous Milk Fat. 3. Influence of Cooling Rate.
789 *Journal of Dairy Science, 88,* 511-526.
790 18. Tippets, M. & Martini, S. (2009) Effect of cooling rate on lipid
791 crystallization in oil-in-water emulsions. *Food Research International, 42,*
792 847-855.

19. Ronholt, S., Kirkensgaard, J. J. K., Pedersen, T. B., Moretensen, K. & Knudsen, J. C. (2012). Polymorphism, microstructure and rheology of butter, Effects of cream heat treatment. *Food Chemistry*, *135*, 1730-1739.

20. Bayés-García, L., Calvet, T., Cuevas-Diarte, M. A., Rovira, E., Ueno, S. & Sato, K. (2015). New Textures of Chocolate are Formed by Polymorphic Crystallization and Template Effects: Velvet Chocolate. *Crystal Growth & Design*, *15*, 4045-4054.

21. Miura, S. & Konishi, H. (2001). Crystallization behaviour of 1,3-dipalmitoyl-2-oleoyl-glycerol and 1-palmitoyl-2,3-dioleoyl-glycerol. *European Journal of Lipid Science and Technology*, *103*, 804-809.

22. Zhang, L., Ueno, S., Miura, S. & Sato, K. (2007). Binary Phase Behavior of 1,3-Dipalmitoyl-2-oleoyl-*sn*-glycerol and 1,2-Dioleoyl-3-palmitoyl-*rac*-glycerol. *Journal of the American Oil Chemists' Society*, *84*, 219-227.

23. Zhang, L., Ueno, S., Sato, K., Adlof, R. O. & List, G. R. (2009). Thermal and structural properties of binary mixtures of 1,3-distearoyl-2-oleoyl-glycerol (SOS) and 1,2-dioleoyl-3-stearoyl-*sn*-glycerol (*sn*-OOS). *Journal of Thermal Analysis and Calorimetry*, *98*, 105-111.

~~23.~~24. Mortimer, R. G. (2005). *Mathematics for Physical Chemistry*. San Diego: Elsevier Academic Press, pp. 326.

~~24.~~25. Perkin Elmer. (1982). Instructions Model DSC-4. Norwalk, Connecticut, USA.

~~25.~~

26. Larsson, K. (1992). On the structure of the liquid state of triglycerides. *Journal of the American Oil Chemists' Society*, *69*, 835-836.

Formatted: German (Germany)

Formatted: Normal, No bullets or numbering

27. Cebula, D. J., McClements, D. J., Povey, M. J. W. & Smith, P. R. (1992). Neutron Diffraction Studies of Liquid and Cristalline Trilaurin. *Journal of the American Oil Chemists' Society*, *69*, 130-136.

28. Corkery, R. W., Rousseau, D., Smith, P., Pink, D. A. & Hanna, C. B. (2007). A Case of Discotic Liquid Crystals in Molten Triglycerides. *Langmuir*, *23*, 7241-7246.

29. Larsson, K. (1972). Molecular arrangement in glycerides. *Fette Seifen Anstrichmittel*, *74*, 136-142.

30. Larsson, K. (1994). *Lipids: Molecular Organization, Physical Functions and Technical Applications*. Dundee: Oily Press, pp. 75-80.

31. Ueno, S., Minato, A., Seto, H., Amemiya, Y. & Sato, K. (1997). Synchrotron Radiation X-ray Diffraction Study of Liquid Crystal Formation and Polymorphic Crystallization of SOS (*sn*-1,3-Distearoyl-2-oleoyl Glycerol. *Journal of Physical Chemistry B, 101*, 6847-6854.

32. ~~Mortimer, R. G. (2005). *Mathematics for Physical Chemistry*. San Diego: Elsevier Academic Press, pp. 326.~~

33. ~~Perkin Elmer. (1982). Instructions Model DSC-4. Norwalk, Connecticut, USA.~~

34. Ostwald, W. Z. (1897). Studien über die Bildung und Umwandlung fester Körper. 1. Abhandlung: Übersättigung und Überkaltung. *Zeitschrift für Physikalische Chemie*, *22*, 289-330.

35. Small, D. M. (1984). Lateral chain packing in lipids and membranes. *Journal of Lipid Research*, *25*, 1490-1500.

Formatted: German (Germany)

842

843

Figure

Click here to download high resolution image

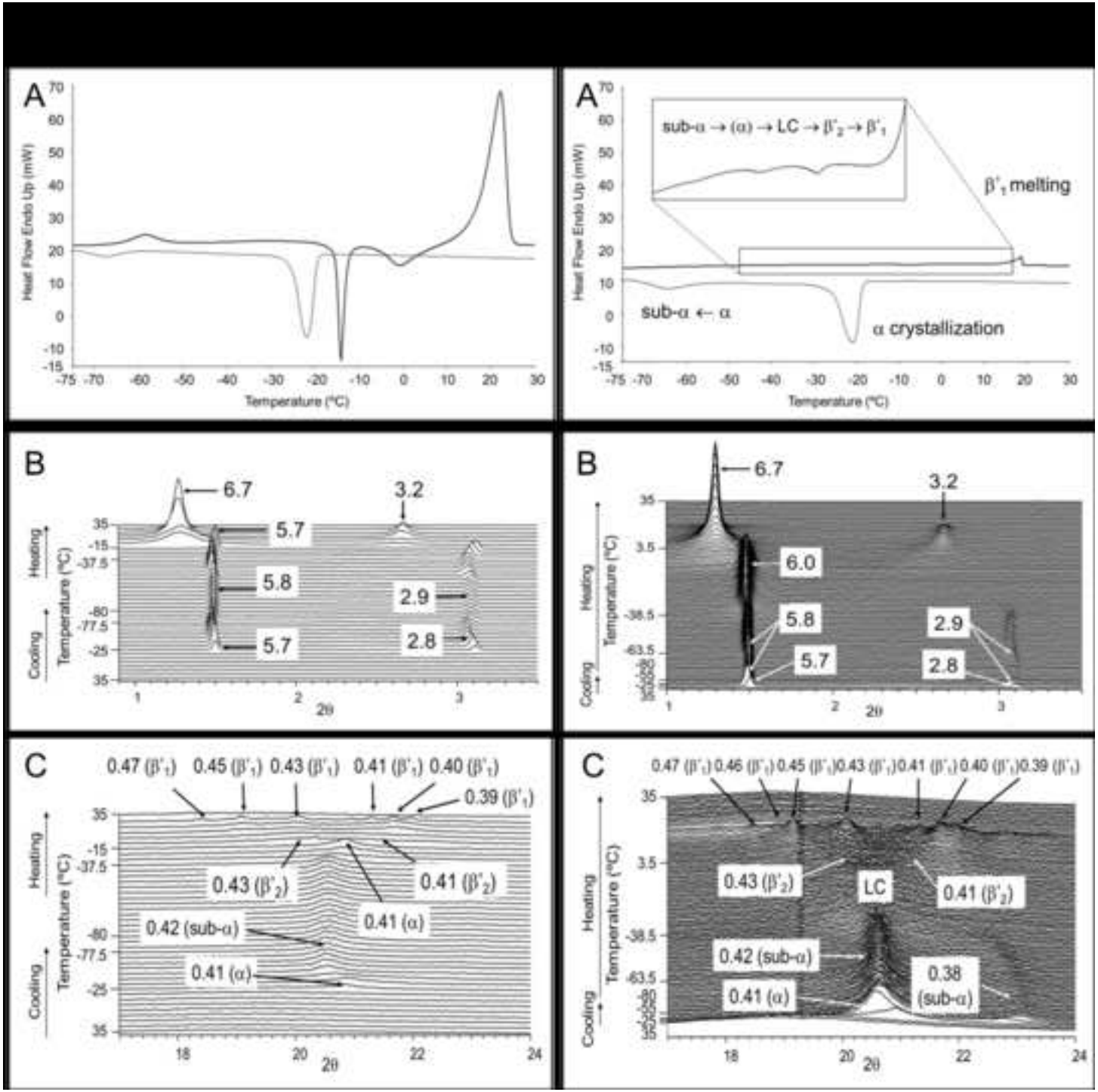

Figure

Click here to download high resolution image

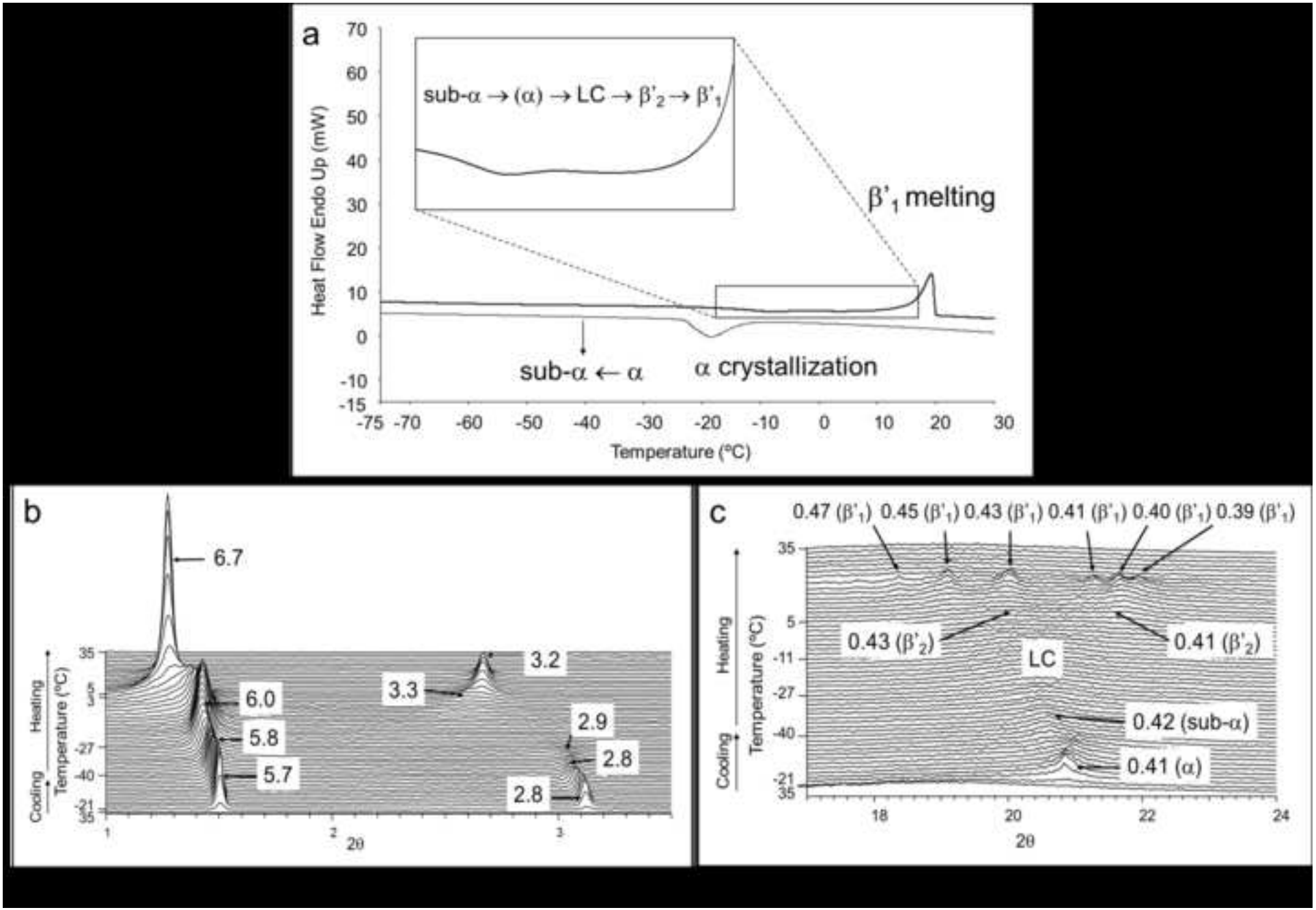

Figure
Click here to download high resolution image

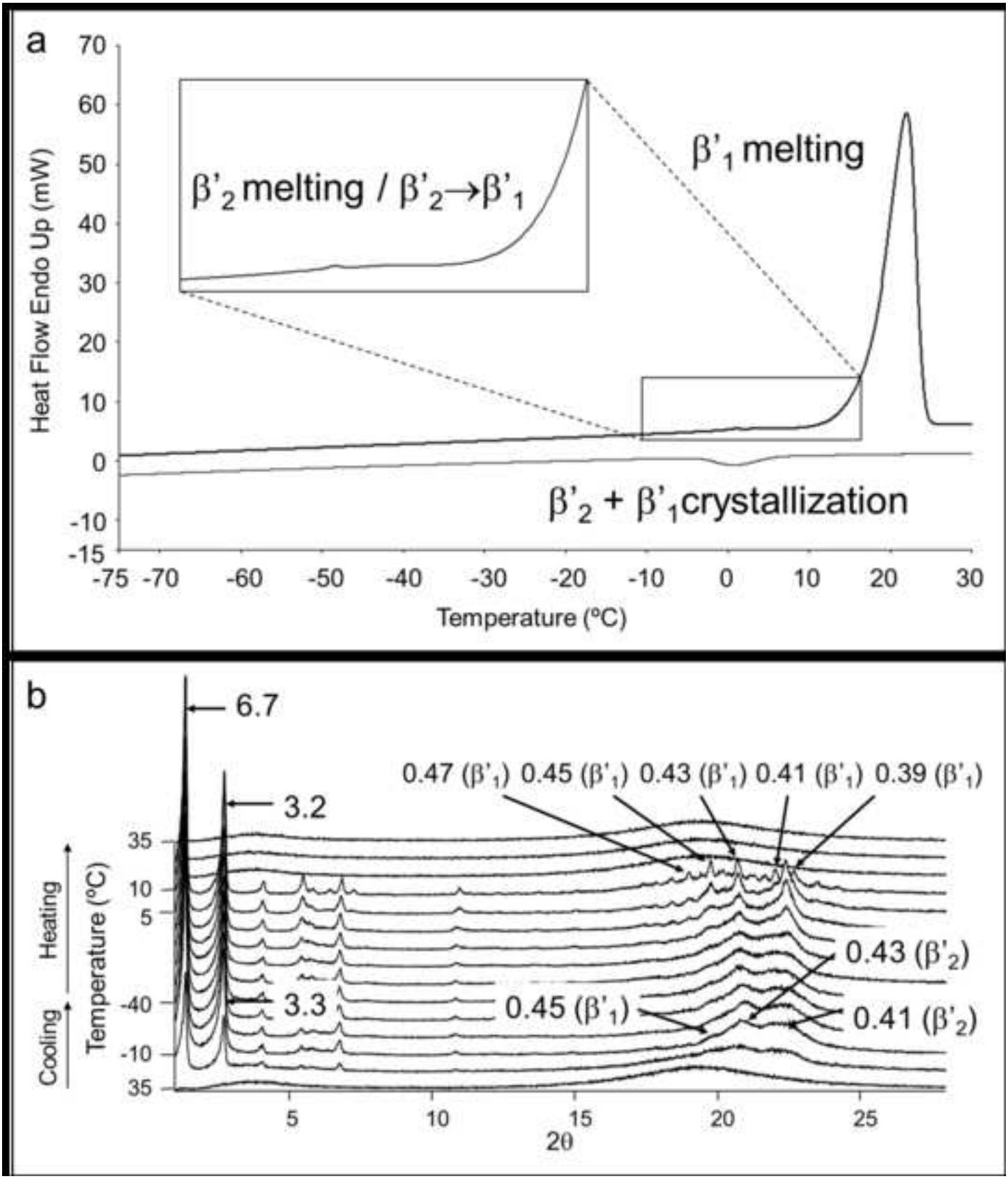

Figure

Click here to download high resolution image

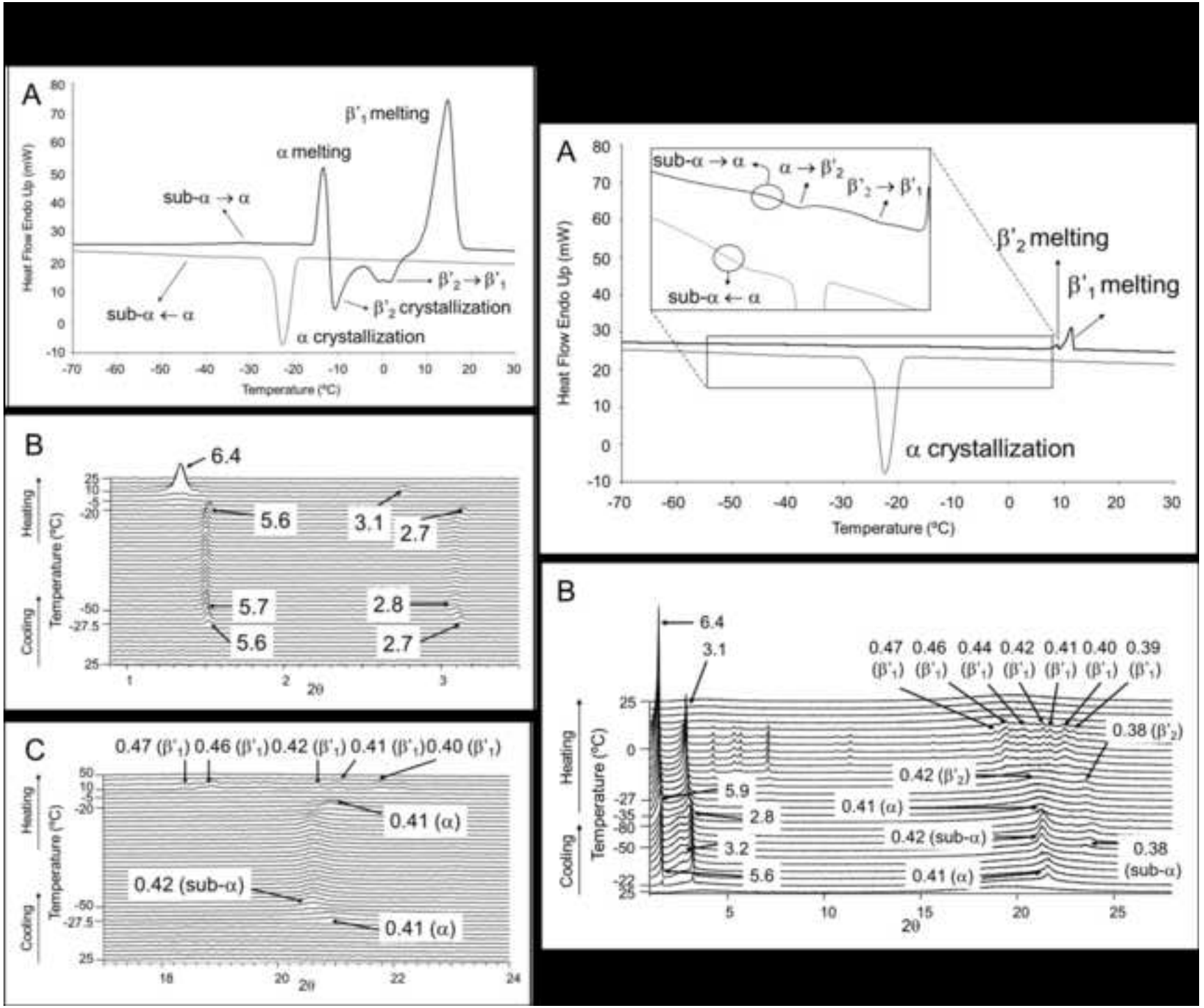

Figure

Click here to download high resolution image

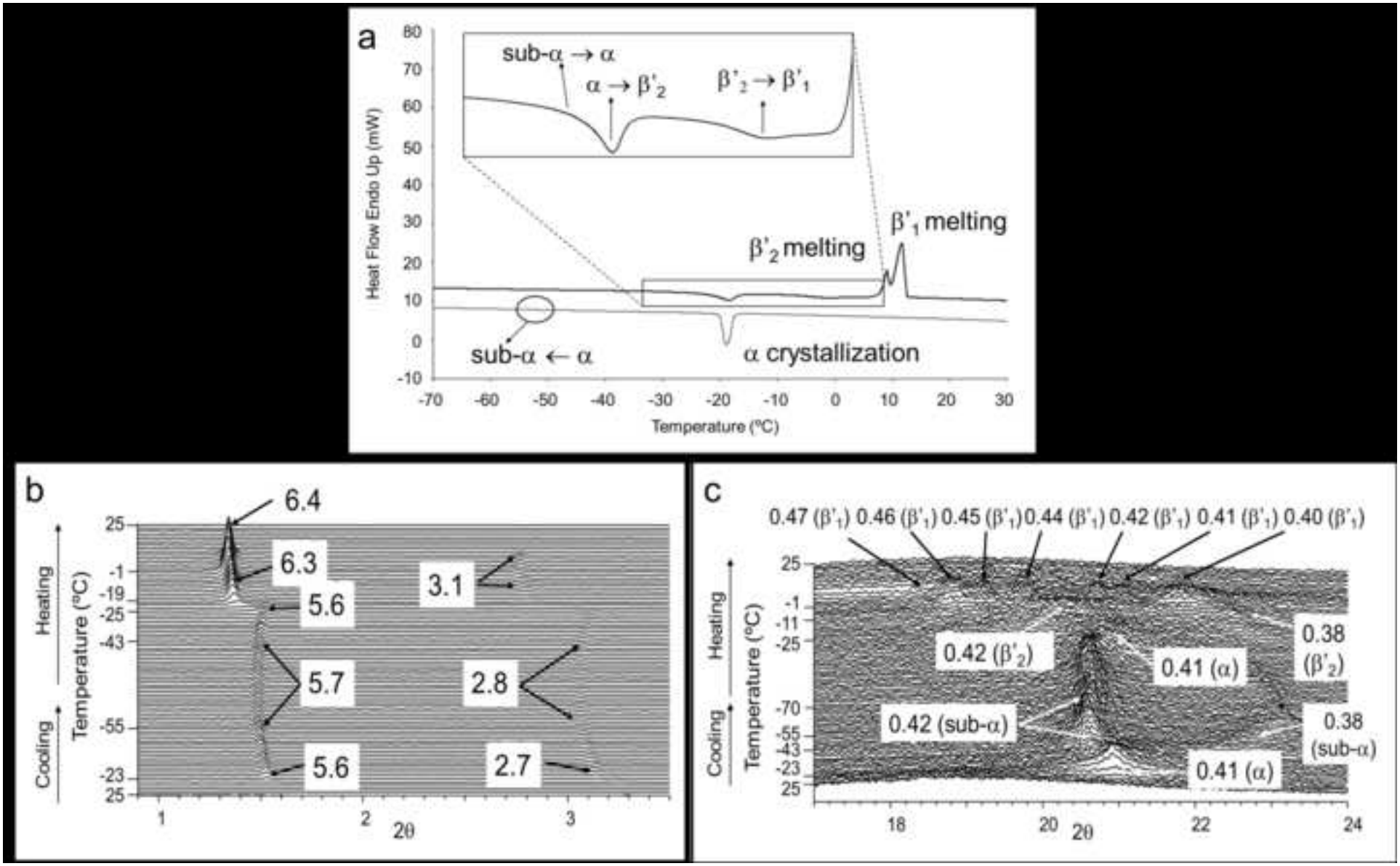

Figure

Click here to download high resolution image

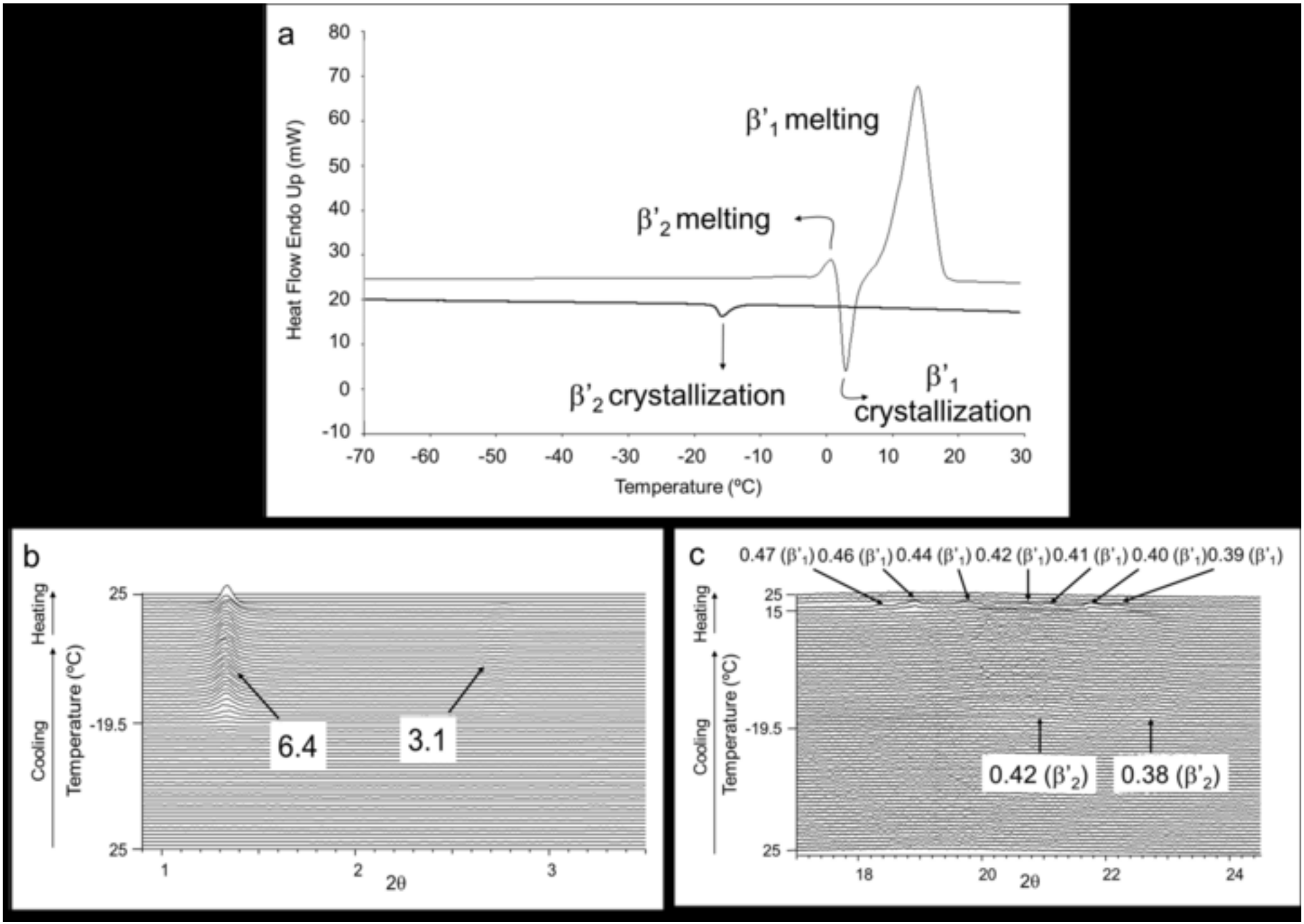

Figure

Click here to download high resolution image

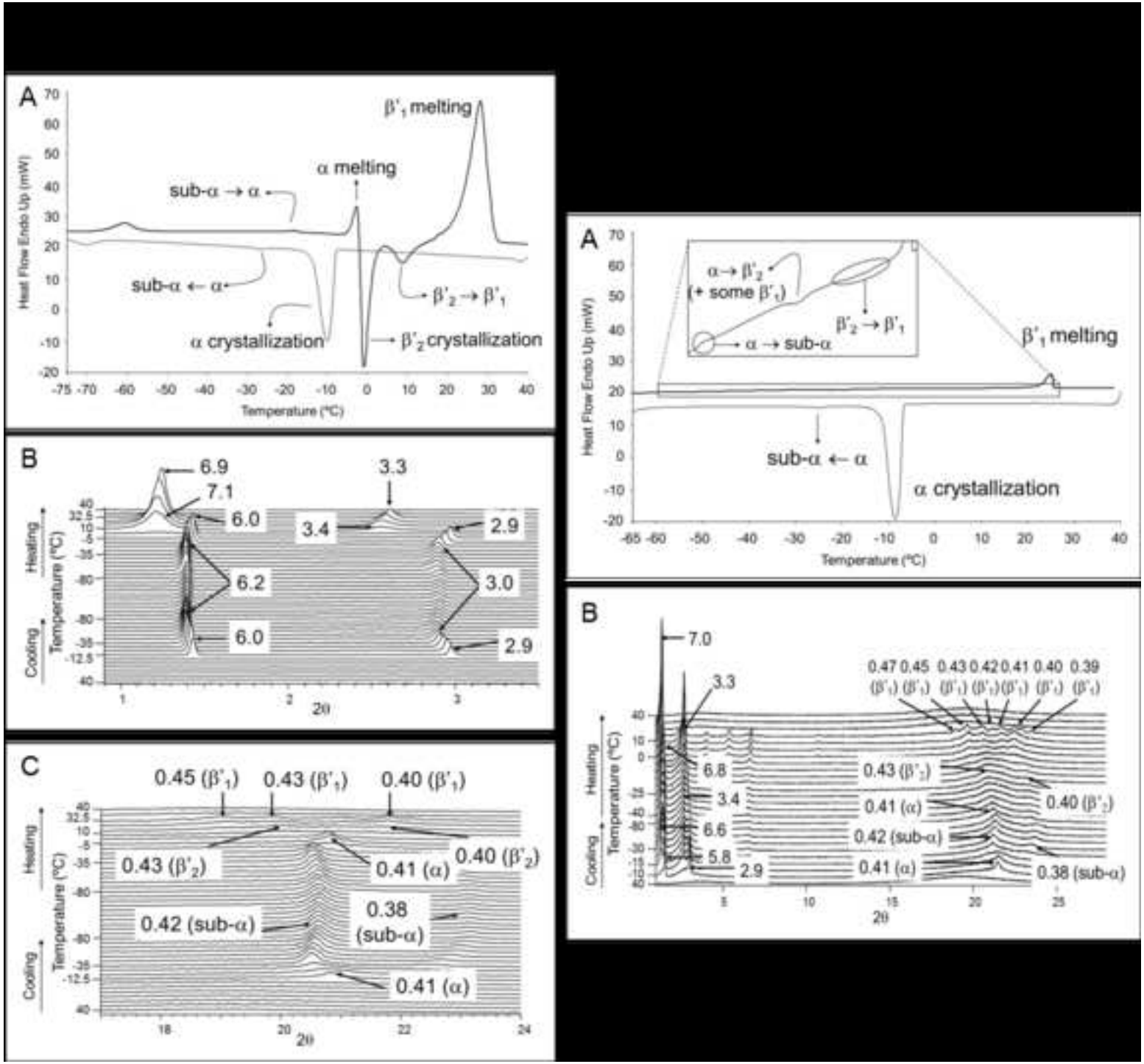

Figure

Click here to download high resolution image

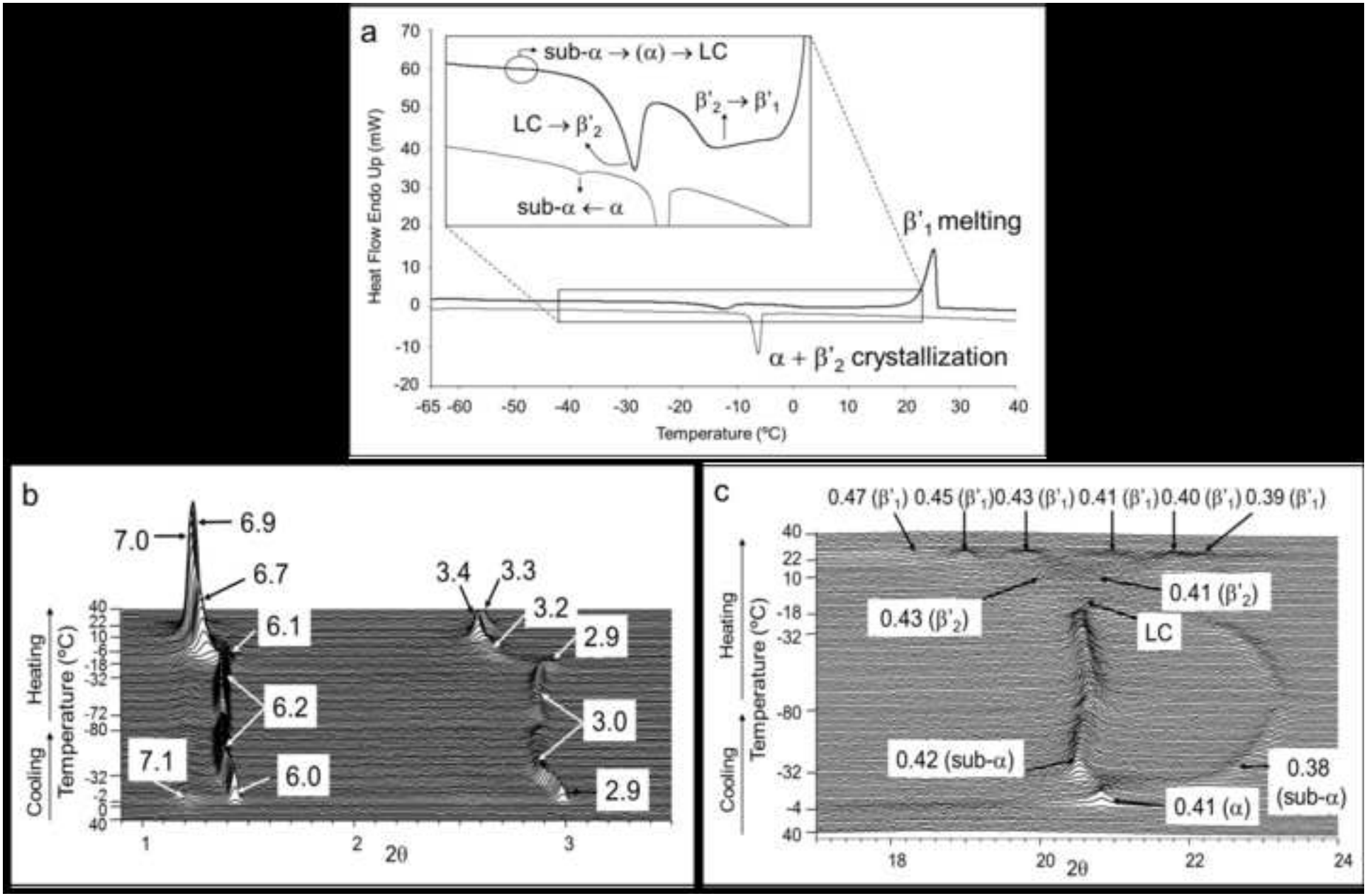

Figure

Click here to download high resolution image

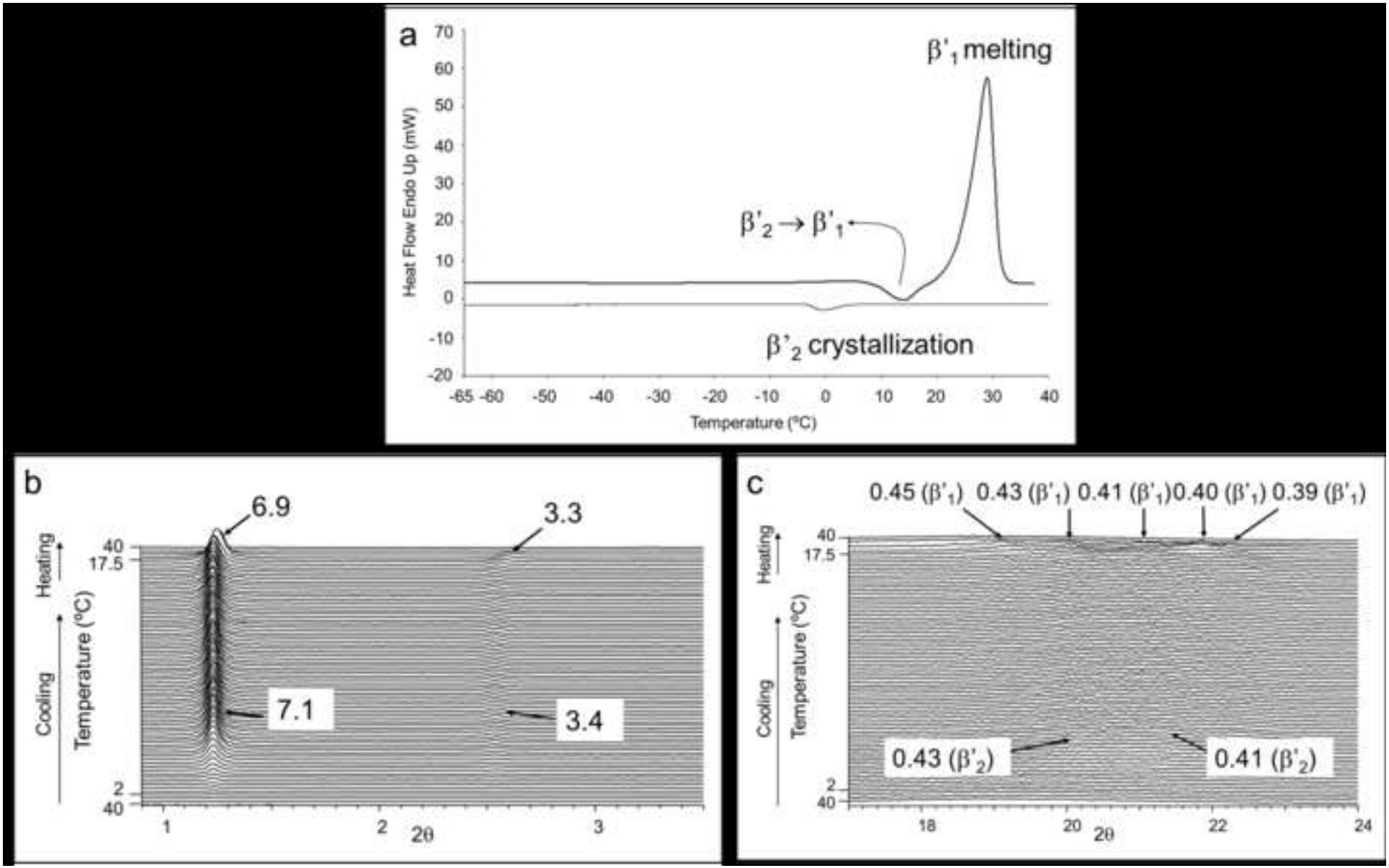

Figure

Click here to download high resolution image

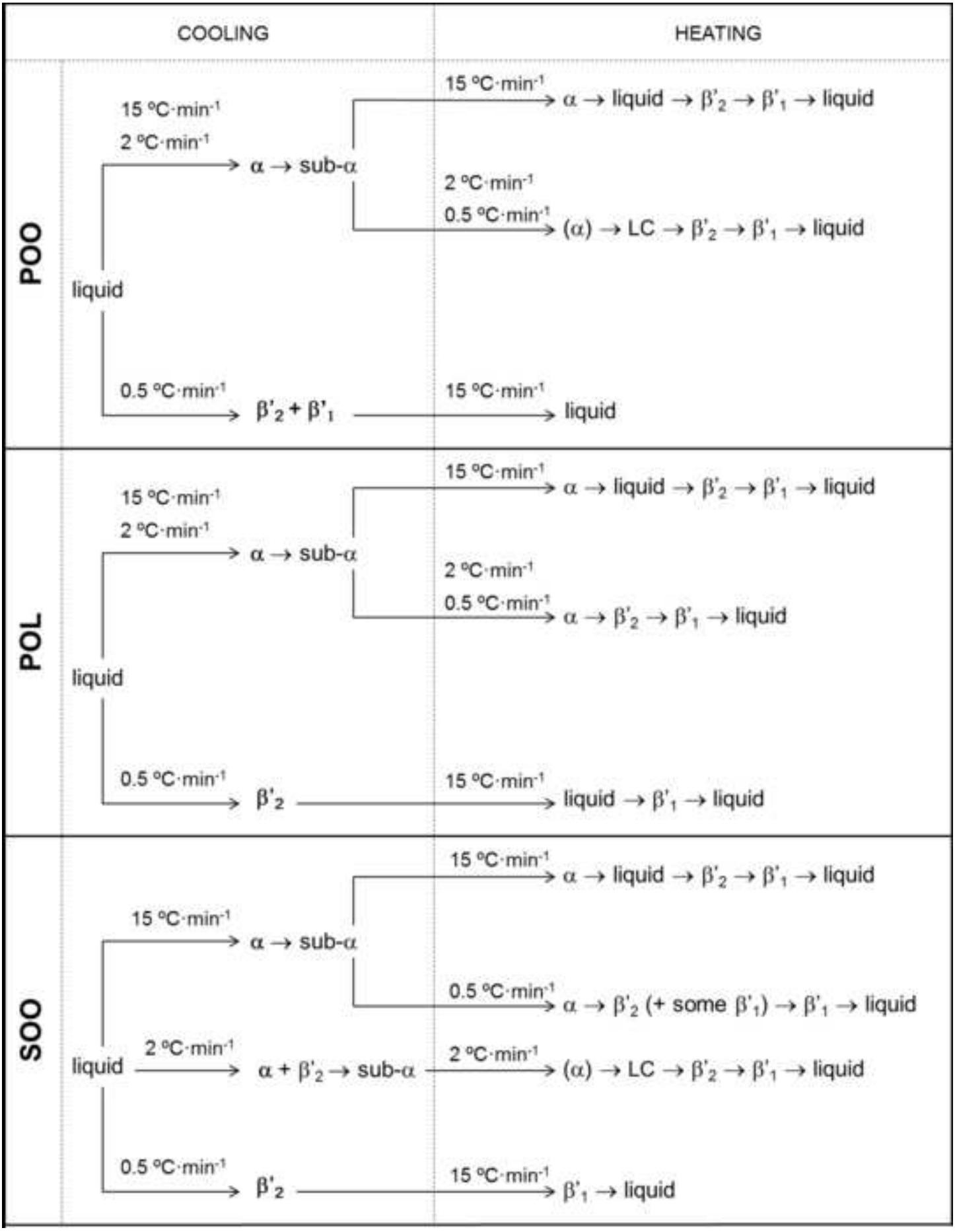

Figure
Click here to download high resolution image

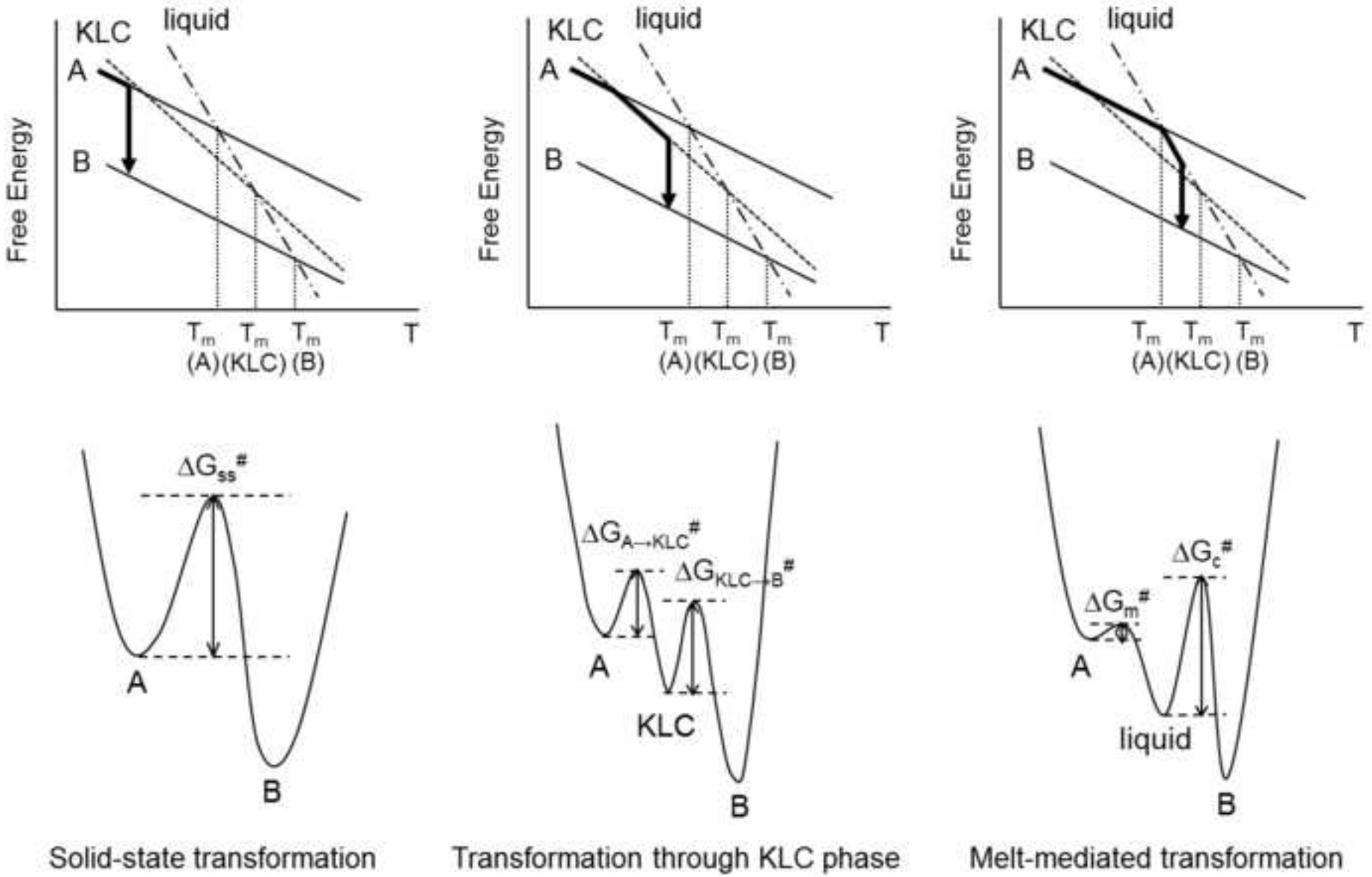

Solid-state transformation

Transformation through KLC phase

Melt-mediated transformation

Figure

Click here to download high resolution image

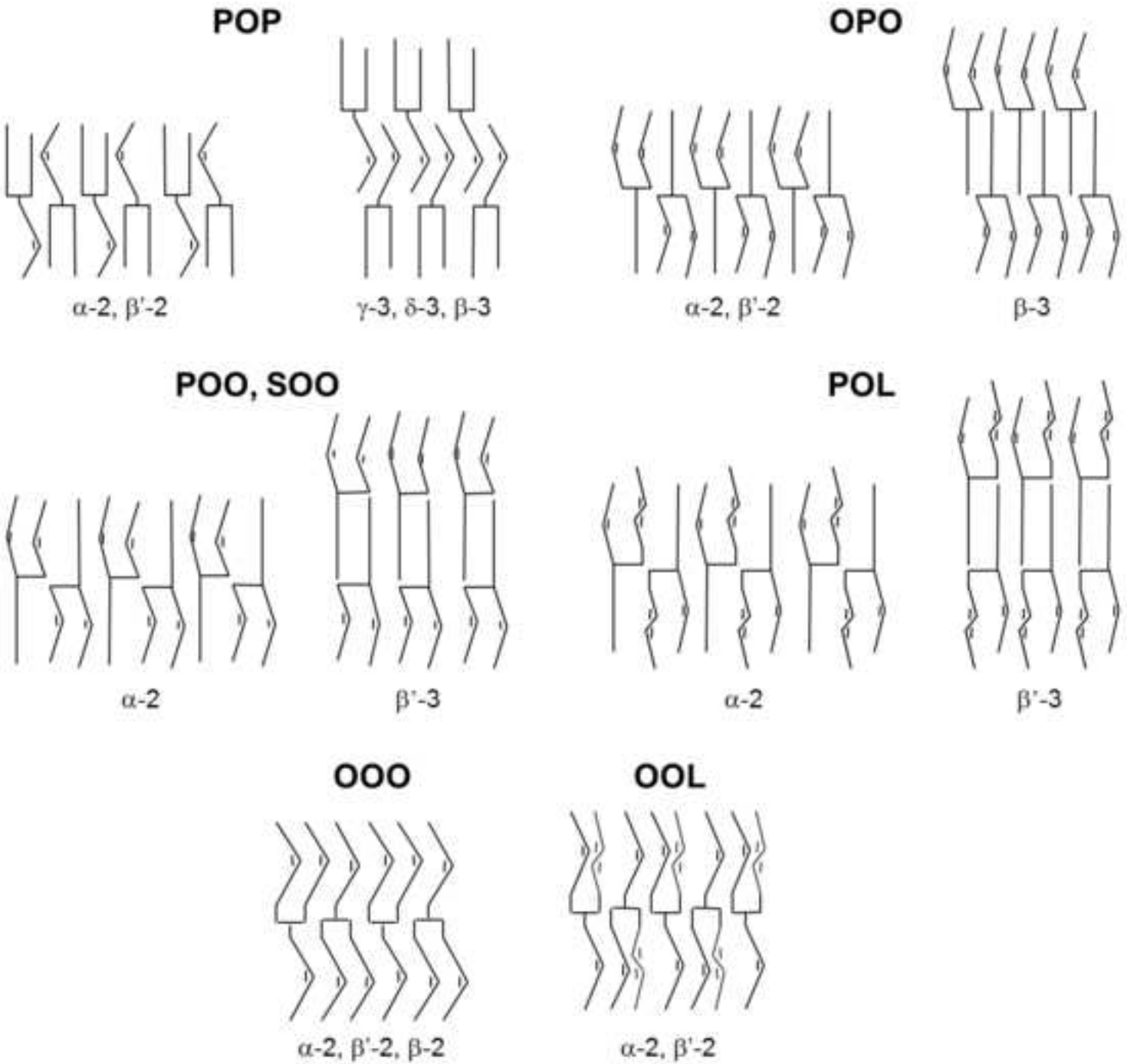

*Graphical Abstract

In Situ Crystallization and Transformation Kinetics of Polymorphic Forms of Saturated-Unsaturated-Unsaturated Triacylglycerols: 1-palmitoyl-2,3-dioleoyl glycerol, 1-stearoyl-2,3-dioleoyl glycerol, and 1-palmitoyl-2-oleoyl-3-linoleoyl glycerol

Laura Bayés-García, Teresa Calvet, Miquel Àngel Cuevas-Diarte and Satoru Ueno

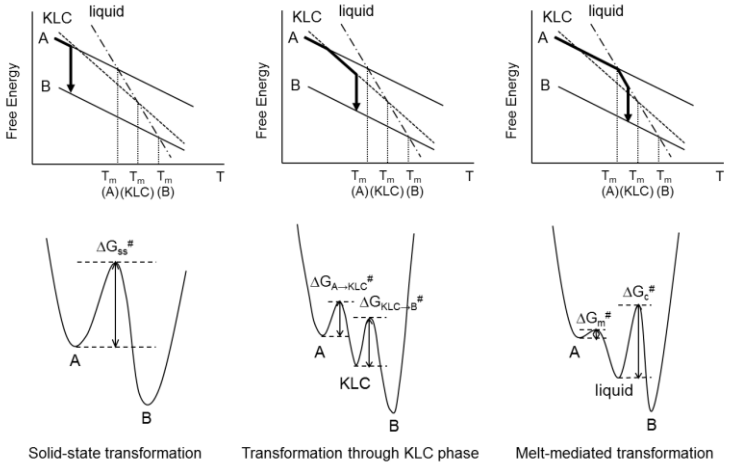

The use of dynamic thermal treatments on the polymorphic crystallization and transformation of POO, POL and SOO is closely related to actual crystallization processes of edible fats, as the occurrence of designed polymorphic forms may be controlled by tailoring the most efficient temperature programs.